Journal for
ImmunoTherapy of Cancer

Engineering CAR-NK cells to secrete IL-15 sustains their anti-AML functionality but is associated with systemic toxicities

Ilias Christodoulou,[1,2] Won Jin Ho,[1] Andrew Marple,[1] Jonas W Ravich,[1] Ada Tam,[1] Ruyan Rahnama,[1,3] Adam Fearnow,[1] Cambrynne Rietberg,[4] Sean Yanik,[4] Elena E Solomou,[2] Ravi Varadhan,[1] Michael A Koldobskiy,[1,3] Challice L Bonifant [ID] [1,3]

[1]Sidney Kimmel Comprehensive Cancer Center, Johns Hopkins University School of Medicine, Baltimore, Maryland, USA
[2]Department of Internal Medicine, University of Patras School of Health Sciences, Patras, Western Greece, Greece
[3]Department of Pediatrics, Johns Hopkins University School of Medicine, Baltimore, Maryland, USA
[4]Department of Pediatrics, University of Michigan, Ann Arbor, Michigan, USA

Correspondence to
Dr Challice L Bonifant;
cbonifa2@jh.edu

ABSTRACT

Background The prognosis of patients with recurrent/refractory acute myelogenous leukemia (AML) remains poor and cell-based immunotherapies hold promise to improve outcomes. Natural Killer (NK) cells can elicit an antileukemic response via a repertoire of activating receptors that bind AML surface ligands. NK-cell adoptive transfer is safe but thus far has shown limited anti-AML efficacy. Here, we aimed to overcome this limitation by engineering NK cells to express chimeric antigen receptors (CARs) to boost their anti-AML activity and interleukin (IL)-15 to enhance their persistence.
Methods We characterized in detail NK-cell populations expressing a panel of AML (CD123)-specific CARs and/or IL-15 in vitro and in AML xenograft models.
Results CARs with 2B4.ζ or 4-1BB.ζ signaling domains demonstrated greater cell surface expression and endowed NK cells with improved anti-AML activity in vitro. Initial in vivo testing revealed that only 2B4.ζ Chimeric Antigen Receptor (CAR)-NK cells had improved anti-AML activity in comparison to untransduced (UTD) and 4-1BB.ζ CAR-NK cells. However, the benefit was transient due to limited CAR-NK-cell persistence. Transgenic expression of secretory interleukin (sIL)-15 in 2B4.ζ CAR and UTD NK cells improved their effector function in the setting of chronic antigen simulation in vitro. Multiparameter flow analysis after chronic antigen exposure identified the expansion of unique NK-cell subsets. 2B4.ζ/sIL-15 CAR and sIL-15 NK cells maintained an overall activated NK-cell phenotype. This was confirmed by transcriptomic analysis, which revealed a highly proliferative and activated signature in these NK-cell groups. In vivo, 2B4.ζ/sIL-15 CAR-NK cells had potent anti-AML activity in one model, while 2B4.ζ/sIL-15 CAR and sIL-15 NK cells induced lethal toxicity in a second model.
Conclusion Transgenic expression of CD123-CARs and sIL-15 enabled NK cells to function in the setting of chronic antigen exposure but was associated with systemic toxicities. Thus, our study provides the impetus to explore inducible and controllable expression systems to provide cytokine signals to AML-specific CAR-NK cells before embarking on early-phase clinical testing.

INTRODUCTION

Acute myelogenous leukemia (AML) is a neoplastic disorder characterized by the accumulation of malignant myeloid precursor cells in the bone marrow. AML has an aggressive clinical course in both adults and children.[1 2] Intensive chemotherapeutic regimens with consolidative hematopoietic cell transplantation (HCT) remain the standard of care, but these treatments can cause significant short-term and long-term toxicities. Moreover, a subset of patients fail to respond to initial treatment or relapse after chemotherapy±HCT. For this reason, targeted therapies with non-overlapping toxicity profiles are aggressively being developed. The alpha chain of the interleukin (IL)-3 receptor (CD123) is highly expressed on both AML blasts and leukemic stem cells,[3 4] and has been shown to be a safe target in clinical trials of immunotherapeutic agents.[5–7] Leukemic stem cells are often resistant to chemotherapy and may be most responsible for disease initiation and relapse.[3] Thus, CD123 targeting therapies could serve as valuable adjunct treatment modalities to achieve and/or sustain remission in high-risk patients with AML.

Adoptive cell transfer is a form of anti-cancer immunotherapy that has promise, and has been successful in the form of chimeric antigen receptor (CAR)–T cell infusions used to treat relapsed/refractory Acute Lymphoblastic Leukemia (ALL).[8] CAR-T cells are also being tested against AML in several clinical trials.[9] CAR-T cell therapies have associated severe toxicities including cytokine release syndrome (CRS), immune effector cell associated neurotoxicity syndrome (ICANS),[10] and CAR-associated hemophagocytic lymphohistiocytosis.[11] All Food and Drug Administration-approved CAR-T cell therapies originate from autologous hematopoietic starting material. The manufacturing of patient-derived T-cell products in the setting of a highly proliferative disease can be challenging.[12 13] Delay in therapy associated with the time required for per-patient CAR-T manufacturing may not be

possible in the setting of uncontrolled AML. In addition, intensive chemotherapy regimens, such as those administered for AML treatment, are associated with poor ex vivo T-cell expansion.[14] Donor T cells can be considered as a product source; however, the infusion of allogeneic T cells is associated with the serious risk of graft-versus-host disease (GVHD).[15]

NK cells are immune effector cells that play a pivotal role as first-line defenders against virally infected or tumor-transformed cells. Though they act with similar cytotoxic mechanisms, NK-cell activation and function are distinct from those of T cells. NK cells express a variety of activating receptors (eg, NKG2D, NKp30, NKp46, 2B4 and CD16)[16 17] that directly interact with cell surface ligands.[16 18] These activating receptors associate with coreceptors (ex. DAP10, CD3ζ and FcεRIγ) to heighten directed cytotoxicity.[17] The use of NK cells for immunotherapy has major advantages over the use of T cells. NK cells do not directly cause GVHD, though they may contribute inflammatory mediators that potentiate pre-existing pathology.[15 19] Thus, they have the potential to be used as an off-the-shelf cellular product that can be manufactured on a large scale and can be readily available to patients. This has the advantage of decreasing production costs and preventing manufacturing associated treatment delays. Adoptive NK-cell transfer has been shown to be safe in clinical trials, without associated CRS or ICANS.[20] Because of this safety profile and the expression of NK activating ligands on AML cells,[18] NK-cell therapy has been tested in clinical trials. However, when used as AML treatment, NK-cell adoptive transfer induces only transient remission, and additional therapies are needed to achieve durable responses.[21–24]

In this study, we engineered NK cells to express CARs with intracellular (IC) domains rationally designed as those predicted to enhance NK-cell antitumor functionality. We demonstrate that NKs expressing CARs targeting CD123 show potent antigen-dependent activation and cytotoxicity. We find CAR expression to be stable and high across a panel of tested receptors incorporating NK-specific activating and costimulatory molecules, with optimal functionality associated with 2B4.ζ and 4-1BB.ζ containing CARs. CAR-NK cells did not demonstrate improved expansion or persistence when compared with unmodified NK cells in vivo. We therefore added constitutive IL-15 secretion to our CAR-NK cells and observed that this supported an activated phenotype that led to enhanced expansion and antitumor cytotoxicity. NK-cell activation translated to improved NK-cell persistence and expansion in vivo. However, constitutive cytokine secretion was also associated with severe toxicity in one animal model. Prior to clinical translation, alternate strategies to activate cytokine signaling in CAR-NK cells should be investigated with a focus to include safety.

METHODS
Details about cell lines, determination of vector copy number (VCN), cytotoxicity assays, cytokine secretion measurement, and RNAseq library preparation and alignment are provided in online supplemental methods.

CAR generation
CAR transgenes were designed using the CD123-specific single chain variable fragment (scFv, 26292)[25] sequence and the hinge (H), transmembrane (TM), and IC domains indicated in figure 1A. Sequences were synthesized (GeneArt, Thermo Fisher Scientific) and subcloned into pSFG retroviral vectors. All sequences were validated by Sanger sequencing (Johns Hopkins Genetic Resources Core Facility).

CAR-NK-cell production
Healthy donor peripheral blood mononuclear cells (Anne Arundel Medical Blood Donor Center, Annapolis, Maryland, USA; Carter Bloodcare, Woodway, Texas, USA) were isolated by Ficoll density gradient centrifugation and depleted of T cells using CD3 microbeads (Militenyi Biotec, Cologne, Germany). The remaining cells were stimulated on day (D)0 with lethally irradiated K562 feeder cells[26] expressing membrane bound IL-15 and 4-1BB ligand at a 1:1 ratio. Cells were maintained in SCGM media (CellGenix, Freiburg, Germany) supplemented with 10% fetal bovine serum, 2 mmol/L GlutaMAX (Thermo Fisher), and 200 IU/mL human interleukin (hIL)-2 (Biological Resources Branch Preclinical Biorepository, National Cancer Institute, Frederick, Maryland, USA). NK-cell purity was verified with flow cytometry using fluorophore conjugated antibodies against CD56 and CD3 (online supplemental table 1). NK cells were transduced on D4 of culture using transiently produced replication incompetent RD114 pseudotyped retroviral particles immobilized on RetroNectin (Clontech Laboratories, Palo Alto, California, USA).

Flow cytometry
Antibodies for NK and cancer cell identification targeted CD56 and CD33 (AML cell lines) or CD19 (Raji) markers. A detailed list of all antibodies, including those used for the evaluation of immune cell phenotype is in online supplemental table 1. CAR expression analysis was performed using incubation with His-tagged recombinant CD123 protein (SinoBiological, Beijing, China) and secondary staining with αHis-PE or αHis-APC (BioLegend, San Diego, California, USA). Dead cells were excluded from analysis using LIVE/DEAD Fixable Viability Stains 780 or 575V (BD Biosciences, Franklin Lakes, New Jersey, USA). Cell enumeration was performed with CountBright counting beads (Thermo Fisher). Human Fc receptors were blocked using Human TruStain FcX (BioLegend). In samples stained with multiple BD Horizon Brilliant reagents, Brilliant Stain Buffer Plus (BD Horizon) was used. Compensation was performed with UltraComp eBeads Compensation Beads (Thermo Fisher). Cell surface antigens were quantified using microspheres of
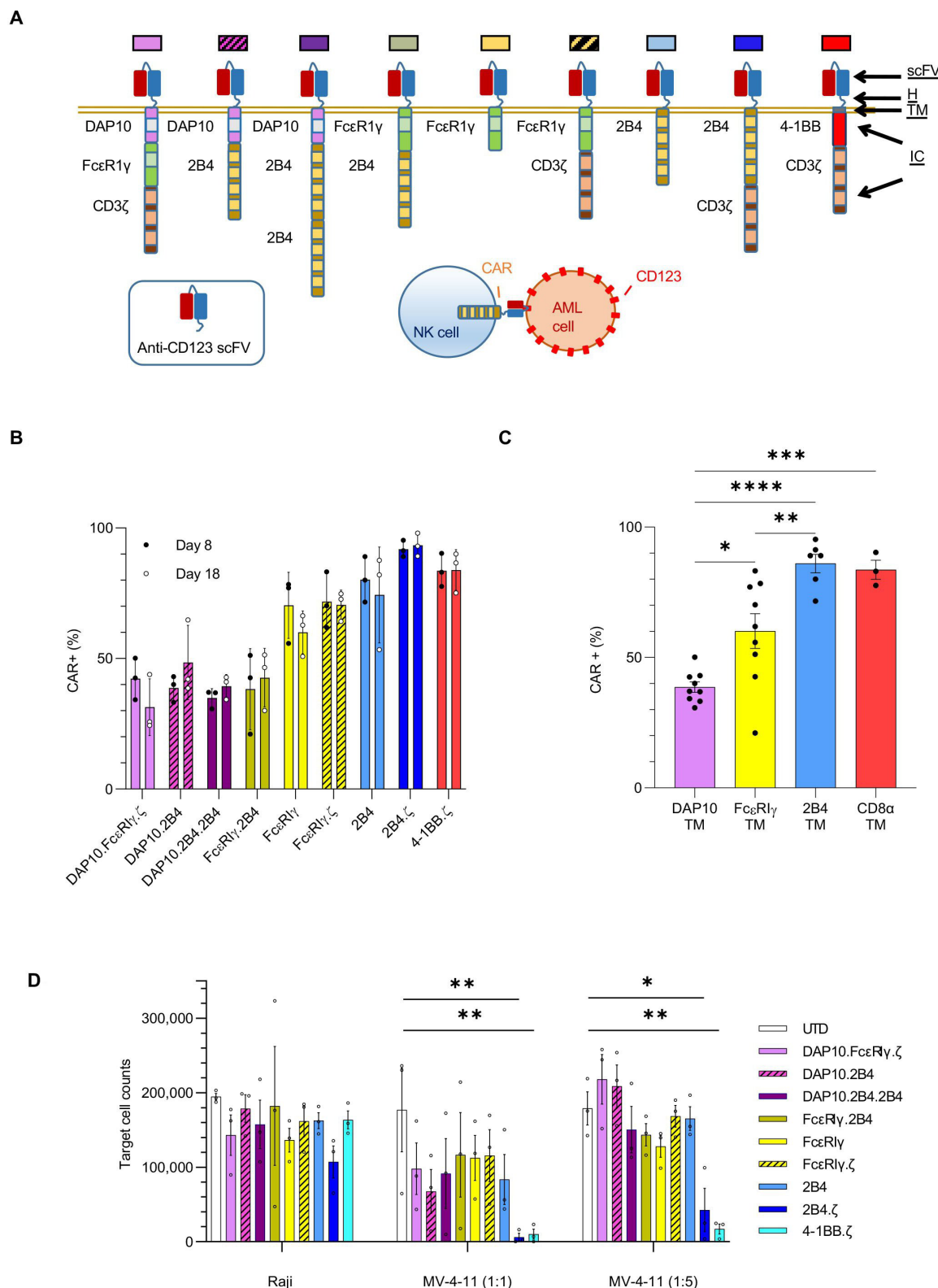
Figure 1 NK cells engineered with anti-CD123 CARs have antigen-specific functionality. (A) Schema of CAR design. All CARs bind CD123 via an extracellular scFv. The H, TM and IC domains of the CARs are as indicated. Colored boxes represents each particular CAR with colors carried through each figure. (B) Percentage (%) of CAR(+) NK cells detected on D8 and D18. (C) Bar plot comparing the percentage of CAR(+) NK cells with indicated TM domains on D8. (D) Absolute number of target cells measured after 72 hours of coculture with indicated NK cells. Initial target cell count was 100 000 in 1:1 and 250 000 in 1:5 E:T ratio conditions. Each bar representative of the mean±SEM; each dot is representative of individual NK cell donor. n=3 donors. *P<0.05, **P<0.01, ***P<0.001, ****P<0.0001. AML, acute myelogenous leukemia; CAR, chimeric antigen receptor; D, day; E:T, effector:target; H, hinge; IC, intracellular; NK, natural killer; ScFv, single-chain variable fragment; TM transmembrane; UTD, untransduced.

the Quantum APC Molecules of Equivalent Soluble Fluorochrome kit (Bangs Laboratories, Fisher, Indiana, USA). All samples were acquired on FACSCelesta or FACSymphony Cell Analyzers (BD Biosciences) and analyzed with FlowJo software V.10.6.1 and V.10.7.2. Cell sorting was performed on FACSMelody (BD Biosciences).

Immunophenotype analysis

Two different panels (A and B) were used for evaluation of NK-cell receptors and one panel (C) for receptor ligands. Data analysis of the multiparameter panels A and B was performed in R V.3.6.2. The median marker intensities were transformed using arcsinh (inverse hyperbolic sine) with cofactor 150.[27] Non-linear dimensionality reduction on randomly selected 500 data points per sample of each panel was performed using uniform manifold approximation and projection (UMAP).[28] NK-cell clusters were identified with the FlowSOM V.1.18.0 algorithm, and 40 different metaclusters were generated per panel.[29] Subsequently, we manually merged hierarchically neighboring clusters similar in biology and median marker intensities. Panel A clusters do not correlate with the ones in panel B.

Serial stimulation assay

NK cells were stimulated daily with MV-4-11 cells at a 1:1 effector:target (E:T) ratio in G-rex plates (Wilson Wolf, New Brighton, Minnesota, USA) for a total of 10 days. NK-cell proliferation and cytotoxicity was measured using flow cytometric analysis. Percent (%) cytotoxicity was calculated based on the target cell numbers on the day of (Y) and the day after (X) stimulation using the formula $100 \times (X-Y)/(Y)$. Cell phenotype was evaluated at baseline, on the 1st (12 hours) and the 10th (D10) days.

RNA sequencing

On D10 of serial stimulation, coculture was depleted first of dead cells using the Dead Cell Removal Kit and next of leukemia cells with CD33 microbeads (Militenyi). NK-cell purity was verified with flow cytometry using fluorophore-conjugated CD56 and CD33 antibodies. RNA was extracted from NK cells using the RNeasy Mini Kit (Qiagen, Hilden, Germany) and RNAseq was performed (online supplemental methods). Differential expression analysis and statistical testing were performed using DESeq2 software.[30] Mice were injected with 1×10^6 MV-4-11 cells modified

Xenograft mouse model

All animal studies were carried out under protocols approved by the Johns Hopkins Institutional Animal Care and Use Committee. NSG (NOD.*Cg-Prkdc*[scid]*Il2rg*[tm1Wjl]/SzJ) mice 6–8 weeks old were obtained from an internal colony that originated from the Jackson Laboratory (Bar Harbor, Maine). Mice were injected with 1×10^6 MV-4-11 cells modified for stable firefly luciferase (ffLuc) expression[31] or 5×10^4 MOLM-13.ffLuc cells[32] via tail vein on D0. NK-cell treatment was administered on D7 (10×10^6 cells) or D4, 7, and 10 (3×10^6 cells each). Mice were given D-luciferin (3 mg) by intraperitoneal injection, and

bioluminescence (BL) was measured using IVIS Spectrum (In Vivo Imaging System). Data were analyzed using Living Image Software V.4.7.3 (PerkinElmer, Waltham, Massachusetts, USA). When indicated, peripheral blood (PB) was drawn via facial vein; red blood cells were lysed with eBioscience RBC Lysis Buffer (Thermo Fisher); and the remaining cells were analyzed with flow cytometry. Bone marrow and spleen were harvested, and tissues were analyzed with flow cytometry. Analysis of PB for cytokines (hIL-15, hTumor Necrosis Factor (TNF)-α, mouse interleukin (mIL)-6, and mIL-1β) was performed with ELISA (R&D Systems). Mice were euthanized when they exhibited >20% weight loss, hind limb paralysis, or moribund state as per protocol guidelines.

Statistical analysis

All statistical analyses was performed using GraphPad Prism Software V.9.2.0. Our comparisons included more than three groups and ordinary one-way or two-way analysis of variance (ANOVA) corrected using the method of Bonferroni. Data with variance of several logs of magnitude were log transformed ($Y=log(Y)$) before analysis with ANOVA. Survival of mice was estimated by the Kaplan-Meier method, and differences in survival between groups were calculated by log-rank (Mantel-Cox) test.

RESULTS

CD123-CARs are highly expressed on the NK-cell surface

We considered NK-cell biology in our design of eight different NK-tailored CARs (figure 1A) to complement the common 4-1BB.ζ CAR.[33 34] All CARs are composed of an extracellular scFv targeting CD123.[25] The H, TM, and IC portion of our CARs consisted of different combinations of activating coreceptors DAP10 and FcεRIγ, the costimulatory receptor 2B4, and the ζ chain of the T-cell receptor (figure 1A). All CARs were expressed stably on the surface of primary human NK cells for at least 2 weeks in culture, with transduction efficiencies ranging from 21% to 98% (figure 1B). Representative flow cytometric plots are shown in online supplemental figure 1A). CARs encoding 2B4 or CD8α TM domains demonstrated higher transduction efficiencies (medians 89 (range 53%–98%) and 84 (range 75%–90%), respectively) than constructs containing FcεRIγ or DAP10 TM (medians 62 (range 21%–77%) and 39 (24%–64%), respectively; figure 1B,C). 2B4 and CD8α TM domains also conferred optimal CAR surface density as estimated by comparative mean fluorescence intensities (MFIs±SEM: 2B4-TM 2158±242, CD8α-TM 3254±970, FcεRIγ-TM 827±151, DAP10-TM 366±23; 2B4 and CD8α vs DAP10: p<0.0001, 2B4 vs FcεRIγ: p<0.01, CD8α vs FcεRIγ: p<0.0001, FcεRIγ vs DAP10: ns; online supplemental figure 1B). CAR-NK cells expanded from 70-fold to 213-fold within 18 days of ex vivo culture with no significant differences between generated CAR-NK-cell populations (online supplemental file 3).

CD123-CAR NK cells have antigen-specific anti-AML activity in vitro

We evaluated the target specificity of our CAR-NK cells using the CD123-positive MV-4-11 and CD123-negative Raji cell lines. When challenged with MV-4-11 in coculture assays, all CAR-NK cells responded with enhanced cytokine secretion above that seen when using unmodified NK cells under identical conditions (mean percent (%) change of interferon gamma (IFN-γ) secretion; CAR-NKs (range): 65%–313% vs unmodified: 14%; online supplemental figure 2). There was no difference in cytokine production of CAR(+) and CAR(−) NK cells after coculture with CD123(−) targets (online supplemental figure 2). Next, we assessed CAR-NK-cell cytotoxicity against CD123(+) target cells in 72-hour coculture assays. We found that CARs with 2B4 or 4-1BB costimulatory and TCRζ signaling domains endowed NK cells with the greatest cytolytic activity against MV-4-11 at both 1:1 (mean % cytotoxicity±SEM: 2B4.ζ 93.8±5%, 4-1BB.ζ 89.9±6.8%) and 1:5 E:T ratios (82.9±11.6% and 93±2.6%, respectively; figure 1D). CD123(−) Raji cells were again used as controls. There was no difference between CAR-NK versus unmodified NK cell-mediated cytotoxicity against Raji cells, confirming specificity (figure 1D).

CD123-2B4.ζ CAR-NK cells have limited anti-AML efficacy in vivo

Given the superior anti-AML activity of 2B4.ζ and 4-1BB.ζ CAR-NK cells in our in vitro assays, we next evaluated their antitumor activity in a xenograft model of human AML. NSG mice were first engrafted with MV-4-11.ffLuc cells,[31] then treated with CAR-NK or unmodified NK cells on D7 (figure 2A). Leukemic growth was measured with serial BL imaging. 2B4.ζ CAR-NK-cell postinjection had transient anti-AML activity, which translated into a significant survival advantage in comparison to other experimental groups (median survival in days: 2B4.ζ vs 4-1BB.ζ 63 vs 56, p<0.01; 2B4.ζ vs unmodified: 63 vs 55, p<0.05) and untreated controls (2B4.ζ vs no treatment 63 vs 58, p<0.01; figure 2B–D). Serial analysis of PB in our animals showed declining NK-cell numbers in all evaluated mice irrespective of infused NK-cell type (figure 2E). Planned bone marrow and spleen examination in a subset of mice demonstrated increasing percentages of leukemia from D15 to D22 in all treatment conditions, despite readily detectable NK cells (online supplemental figure 3). Consistent with BL data, the percentage of leukemic cells was lower in both bone marrow and spleen samples of 2B4.ζ CAR-NK cell-treated mice as compared with mice treated with UTD and 4-1BB.ζ CAR-NK cells (online supplemental figure 3).

## Armoring NK cells with secreted IL-15 enhances anti-AML functionality in vitro

Having demonstrated that 2B4.ζ CAR-NK cells have anti-AML cytolytic capacity with short persistence, we next explored if transgenic expression of IL-15 in CAR-NK cells would support sustained anti-AML activity. To accomplish this, we cloned a sequence encoding human IL-15 downstream of an Internal Ribosome Entry Site (IRES) element into our 2B4.ζ CAR vector. We simultaneously generated a second retroviral vector encoding IL-15 and the fluorescent molecule mOrange as a control with IL-15, but not CAR expression (figure 3A). We verified transduction by measuring VCN per cell (median: 2B4.ζ 10 (range 5.8–14), 2B4.ζ/sIL-15 4.1 (range 3.8–4.7), sIL-15/mOrange 16.6 (range 4.8–19.2); figure 3B). We found no significant difference in VCN/cell or in CAR expression between NK cells transduced with 2B4.ζ or 2B4.ζ/sIL-15 encoding retroviral vectors (range CAR(+): 2B4.ζ vs 2B4.ζ/sIL-15 70%–97% vs 81%–96%, p>0.99, MFI±SEM: 2B4.ζ vs 2B4.ζ/sIL-15 2566±531 vs 2089±424; p>0.99; figure 3C and online supplemental figure 4A). Expression of IL-15 was measured with quantitative reverse transcription (qRT)-PCR (online supplemental figure 4B) and IL-15 secretion was confirmed by ELISA (figure 3D).

We evaluated short-term cytotoxicity of 2B4.ζ/sIL-15 CAR-NKs against the CD123(+) MV-4-11, MOLM-13, and Raji.CD123 cell lines. The parental CD123(−) Raji line was used as a negative control. When compared with 2B4.ζ, the 2B4.ζ/sIL-15 CAR-NKs had higher cytotoxicity against CD123+ targets (figure 3E–G). Both 2B4.ζ and 2B4.ζ/sIL-15 demonstrated antigen-specific cytotoxicity as Raji.CD123 were more effectively killed than parental (CD123−) Raji cells (figure 3G). Target cell CD123 and IL-15Rα expressions were quantified in order to evaluate for any effect of CD123 surface density or IL-15 trans presentation on NK-cell cytotoxicity (online supplemental figure 5A). Differences in measured CD123 surface density did not correlate with observed short-term cytotoxicity, underlining the existence of additional complex mechanisms affecting NK-cell activation. Similarly, differences observed in IL-15Rα expression did not correlate with cytotoxicity (online supplemental figure 5B).

Transgenic expression of IL-15 potentiates the activation, persistence, and long-term cytolytic activity of CAR-NK cells

Using a model of chronic antigen stimulation (figure 4A), we evaluated the immune phenotype of our CAR-NK cells at baseline, after 12 hours, and on D10 of coculture with MV-4-11. Cells were counted daily, and AML was repleted to maintain a 1:1 E:T ratio. We used flow cytometry to measure surface expression of markers in two different panels (panels A and B), then performed hierarchical clustering of NK-cell subsets (figure 4B,C, and online supplemental figure 6). In panel A, we observed similar population distributions in the 2B4.ζ CAR and unmodified NK cells with cluster shifts from earlier (12 hours) to later (D10) time points. Specifically on D10, there was an increase in the percentage of 2B4.ζ and unmodified NK cells populating clusters defined by lower surface expression of activating receptors NKG2D and NKp30 (clusters 19, 25, and 31; figure 4B,C, and online supplemental figure 7). For 2B4.ζ/sIL-15 CAR-NK cells, only minimal
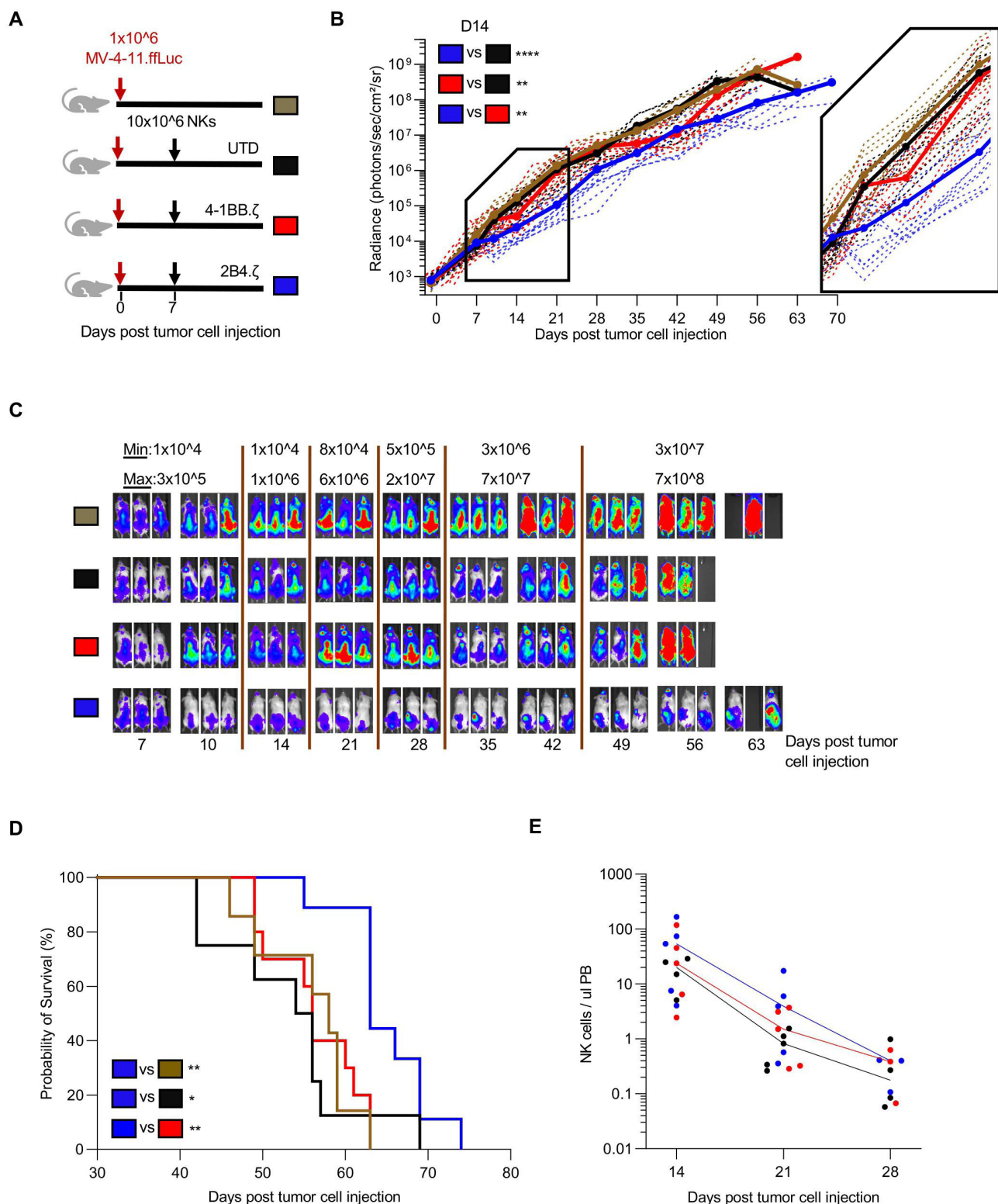
Figure 2 Anti-CD123.2B4.ζ CAR-NKs have transient anti-AML activity in vivo. (A) Schematic of MV-4-11 xenograft model. On D0, NSG mice were injected via tail vein with 1×10^6 CD123(+) MV-4-11 cells that express ffLuc (MV-4-11.ffLuc cells). In treatment groups, 10×10^6 NK cells were administered on D7. Cohorts: UTD/unmodified, 4-1BB.ζ CAR-NK, and 2B4.ζ CAR-NK. (B) Leukemia proliferation was monitored with bioluminescence imaging and was recorded as photons/s/cm²/sr; n=8–12 mice per group. Magnification of D7–D21 shown. (C) Representative images of three mice per condition. Minimum and maximum values of color scale are depicted at the top (min–max). (D) Kaplan-Meier survival analysis of MV-4-11 xenografts (n=8–12 mice per condition). (E) Mouse PB collected at indicated time points and analyzed via flow cytometry. Each dot represents a single mouse. Solid line: median. At later time points, NK-cell count was undetectable for all groups and is not plotted. *P<0.05, **P<0.01, ****P<0.0001. AML, acute myelogenous leukemia; CAR, chimeric antigen receptor; D, day; ffLuc, firefly luciferase; NK, natural killer; PB, peripheral blood; UTD, untransduced.
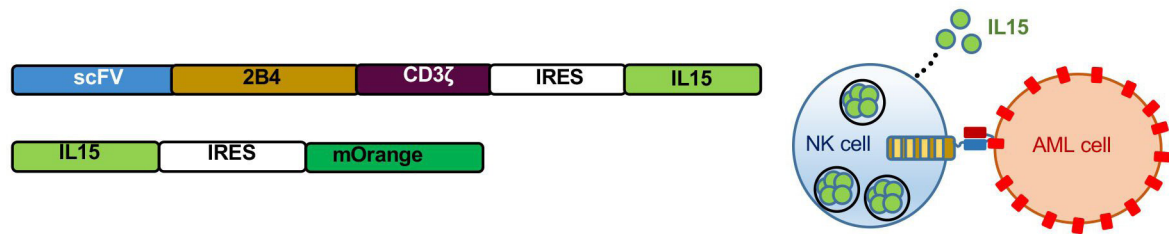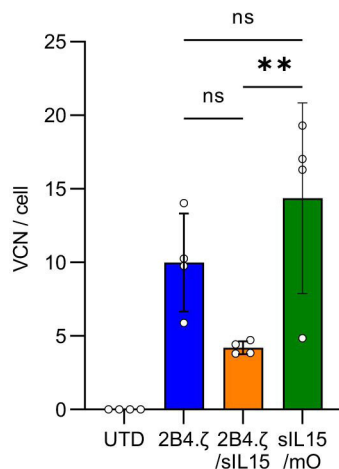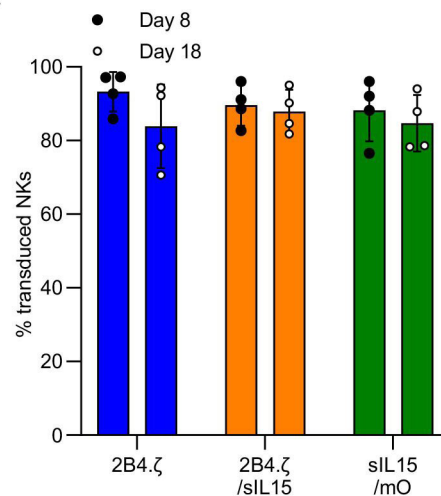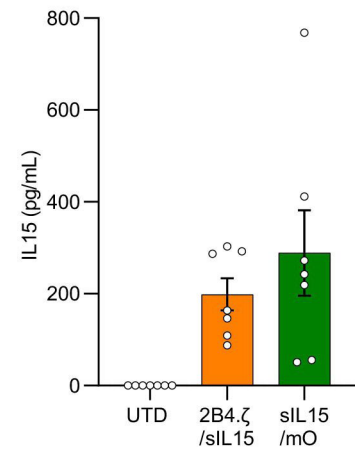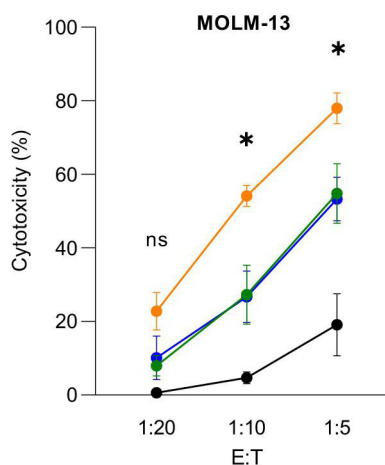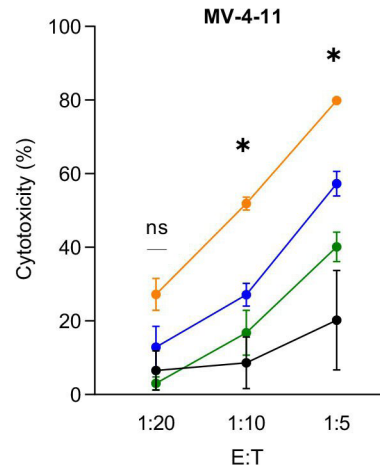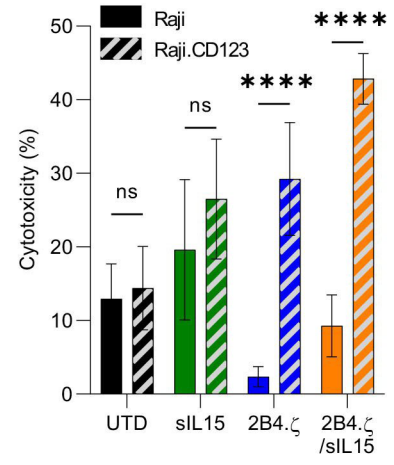
Figure 3 Simultaneous 2B4.ζ CAR expression and IL-15 secretion strengthens NK-cell cytotoxicity. (A) Schema of vectors and IL-15 secretion from CAR-NK cells. (B) Quantification of retroviral VCN in transduced NK cells. UTD NK cells served as negative controls (n=4 donors). (C) Percentage (%) of transduced NK cells in cultures on D8 (black circle) and D18 (white circle, n=4 donors). (D) NK-cell supernatant was used for quantification of IL-15 by ELISA (n=7 biological replicates using four donors). BL-based cytotoxicity assays were performed using the CD123(+) AML cell lines MV-4-11(E) and MOLM-13 (F) with ffLuc expression (n=4 donors). Asterisks indicate 2B4.ζ/sIL-15 versus 2B4.ζ comparison. (G) Bar graph comparing percent (%) cytotoxicity of NK cells against Raji (CD123(−): solid), and Raji (CD123 (CD123(+): diagonal stripe) cancer cell lines at 1:10 E:T ratio (n=4 donors). (B-G) Mean±SEM represented. *P<0.05, **P<0.01, ****P<0.001. AML, acute myelogenous leukemia; BL, bioluminescence; CAR, chimeric antigen receptor; D, day; E:T, effector:target; ffLuc, firefly luciferase; IL, interleukin; NK, natural killer; ns, not significant; ScFv, single-chain variable fragment; sIL, secretory interleukin; UTD, untransduced; VCN, vector copy number.
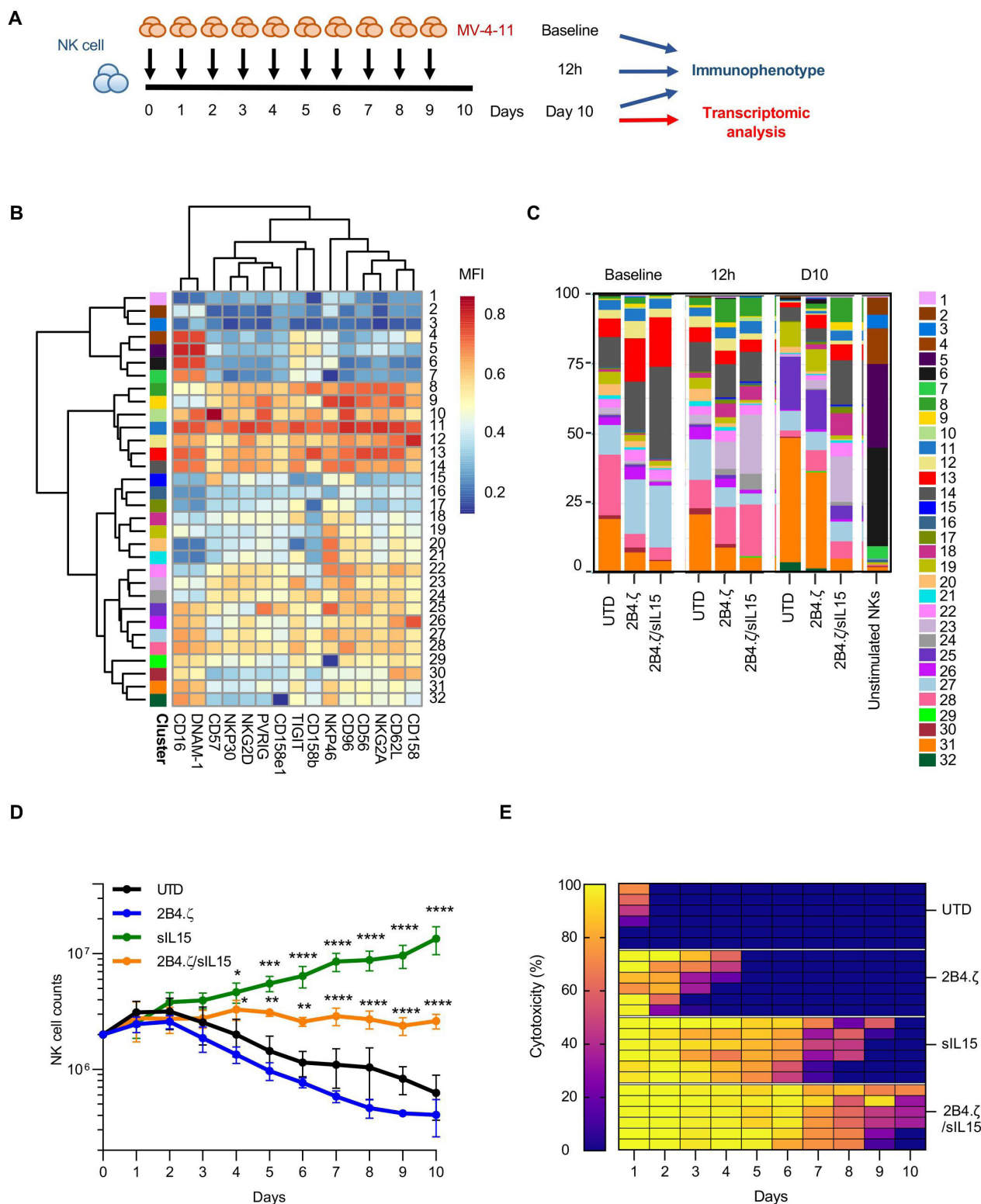
Figure 4 IL-15 maintains NK cell-activated phenotype in a model of chronic antigen stimulation. (A) Schematic representation of our serial stimulation assay. D0 was the day of the initial seeding of the coculture; D1 was the first; and D10 was the last day of cell quantification. Immunophenotypical analysis of effector and target cells performed at baseline (before coculture), 12 hours after first stimulation, and on D10 (n=1 donor). Transcriptomic analysis performed on D10 (n=3 donors). (B) Heatmap of flow cytometry data showing expression of 15 different NK-cell surface markers. Heatmap coloring represents arcsinh transformed median marker intensity. (C) Bar plots of relative abundance of the 32 population subsets found in each sample. (D) NK-cell counts over a period of 10 days. Initial seeding count was two million NK cells (mean±SEM, n=3 donors). Asterisks indicate 2B4.ζ/sIL-15 versus 2B4.ζ and sIL-15 versus UTD comparison. (E) Heat map of the percent (%) NK-cell cytotoxicity. Each column represents the specific day and each row a unique biological replicate (n=3 donors). D, day; IL, interleukin; MFI, mean fluorescence intensity; NK, natural killer; sIL, secretory interleukin; UTD, untransduced.

changes in population density of these subsets were observed on D10 (figure 4B,C). The unique 2B4.ζ/sIL-15 immunophenotype is highlighted by comparison of the MultiDimensional Scaling (MDS, global) and UMAP (cluster-specific) plots in online supplemental figure 8.

Clustering of NK cells based on expression of markers included in our second receptor panel (panel B) again supported the maintained NK-cell activation to D10 in 2B4.ζ/sIL-15 CAR-NK cells (predominant clusters 16, 20, and 26 and minor clusters 11, 13, 14, 15, 21, and 23; online supplemental figures 6–9). Differences were again observed in 2B4.ζ and unmodified NK cells on D10 compared with earlier time points (increasing percentage of cells populating clusters 2, 4, 17, and 18, and decreasing percentages of 14, 16, 20, nd 26; online supplemental figure 6). Clusters 14, 16, 20, and 26 expressed higher levels of LFA-1, CD69, TRAIL, TIM-3, NKG2A, and KLRG1 compared with clusters 2, 4, 17, and 18 (online supplemental figure 9). Negligible differences were observed in PD-1, LAG-3, FASL, 2B4, and NKG2C expression. Taken together, 2B4.ζ/sIL-15 CAR-NKs had a higher percentage of NK cells populating clusters defined by higher surface expression of LFA-1 (adhesion/activation receptor), CD69 (activation marker), TRAIL (death receptor), and TIM-3 (commonly upregulated after NK-cell activation), as well as NKG2A and KLRG1 (inhibitory receptors; figure 4B,C, and online supplemental figures 6–10). Overall, the data from both antibody panels suggest that with continuous antigen stimulation, IL-15 preserves an activated CAR-NK-cell phenotype associated with high cytotoxicity. We also analyzed the expression of NK-cell activating and inhibitory ligands. AML cells expressed high levels of MICA/MICB (NKG2D ligands), CD112 and CD155 (DNAM-1, PVRIG, CD96, and TIGIT ligands) and PDL1 (PD-1 ligand), but not ULBP1 (NKG2D ligand) or galectin-9 (TIM-3 ligand, online supplemental figure 11).

Next, we evaluated NK-cell cytotoxicity and persistence in our model of chronic antigenic stimulation (figure 4A). While unmodified and 2B4.ζ CAR-NK cells sharply diminished in number over the course of this assay, NK cells genetically engineered to express IL-15 (2B4.ζ/sIL-15 and sIL-15) survived throughout the experiment (n=3, figure 4D). As predicted by the short-term cytotoxicity assay, 2B4.ζ CAR-NK cells had high initial anti-AML activity. However, their killing potential decreased as 2B4.ζ CAR-NK-cell counts declined. Cytotoxicity was completely abrogated by D5 (figure 4E). IL-15 activation alone (without CAR expression) also had an early anti-tumor effect that was not sustained. Only the combination of CAR expression and IL-15 secretion led to continued NK cell-mediated anti-AML cytotoxicity (figure 4E and online supplemental figure 12).

NK cells secreting IL-15 exhibit a highly proliferative and activated transcriptomic signature after chronic antigen stimulation

We evaluated the transcriptional programs of our NK cells on the 10th day of continuous antigen stimulation.

NK cells were isolated, and RNA libraries were prepared and used for RNAseq analysis. Samples clustered by IL-15 secretion, with overlap between 2B4.ζ/sIL-15 and sIL-15 conditions. These clearly separated from NK cells that did not secrete IL-15 (UTD and 2B4.ζ, figure 5A). Differential gene expression analysis (DESeq2) of 2B4.ζ/sIL-15 versus 2B4.ζ and sIL-15 versus UTD NKs identified in the IL-15-secreting NK-cell differences in expression of genes in the pathways of DNA replication, cell cycle progression, and NK cell-mediated cytotoxicity (figure 5B,C). Kyoto Encyclopedia of Genes and Genomes (KEGG) enrichment analysis revealed cell cycle progression as the top-ranked pathway for both comparisons (figure 5C). No biologically relevant pathways were found to be significantly enriched when comparing IL-15-secreting CAR-NK cells to non-CAR sIL-15 NKs (online supplemental figures 13A,B). Hierarchical clustering of differentially expressed genes also revealed upregulation of genes involved predominantly in cell cycle progression, chemokine, and cytokine signaling in IL-15-secreting NK conditions (figure 5D and online supplemental table 2). We used this dataset to evaluate differential expression of molecules of biological relevance. 2B4.ζ/sIL-15 and sIL-15 NK cells had higher expression of genes encoding for NK activating receptors (*NCR2* (NKp44), *NCR3* (NKp30), *KLRC2* (NKG2C), *KLRC4-KLRK1* (NKG2D), *CD226* (DNAM-1), and *FCGR3A* (CD16)), adaptor molecules (*FCER1G* (FcεRIγ)), death receptor ligands (*TNFSF10* (TRAIL)), granzyme (granzyme A (*GZMA*), proinflammatory cytokines and chemokines (*IFNG* (IFN-γ), *CCL1*, *CCL3*, *CCL4*, *XCL1*, *XCL2*, and *CCL3L3*), activation markers (*CD69*), proliferation markers (*MKI67* (Ki-67)), antiapoptosis regulators (*BCL2*), and adhesion molecules (*ITGB2* (integrin-β2), *CD2*, and *CD53*; figure 5E and online supplemental figure 13C). We also observed upregulation of select inhibitory receptors (*NKG2A*, *CEACAM1*, and *LILRB1*) including inhibitory killer Ig-like receptors (KIRs; *KIR2DL1*, *KIR2DL2*, *KIR2DL3*, *KIR2DL4*, and *KIR3DL1*) as well as 'checkpoint' molecules (*HAVCR2* (TIM-3) and *TIGIT*, figure 5E and online supplemental figure 13C). KIRs are subject to extensive regulatory splicing and there is an inability to distinguish KIR with identical extracellular domains but functionally disparate IC tails by flow cytometry, making transcriptional analysis necessary and complementary for study of KIR expression. Analysis of the chemokine receptor expression showed upregulation of *CCRL2*, *CCR1*, *CCR5*, and *CCR6* with similar or lower expression of *CX3CR1*, *CXCR3*, and *CXCR4* in IL-15-secreting NKs (online supplemental figure 13C).

Constitutive IL-15 expression improves NK cell in vivo persistence but causes lethal toxicity

We next evaluated IL-15-secreting NK cells in two AML xenograft models. In our first experiment, we used our MV-4-11 xenograft model (figure 2A) and our previous NK-cell dosing regimen (online supplemental figure 14A). Surprisingly, MV-4-11 engrafted mice treated with 10×10^6 IL-15-secreting NK cells had early mortality (median
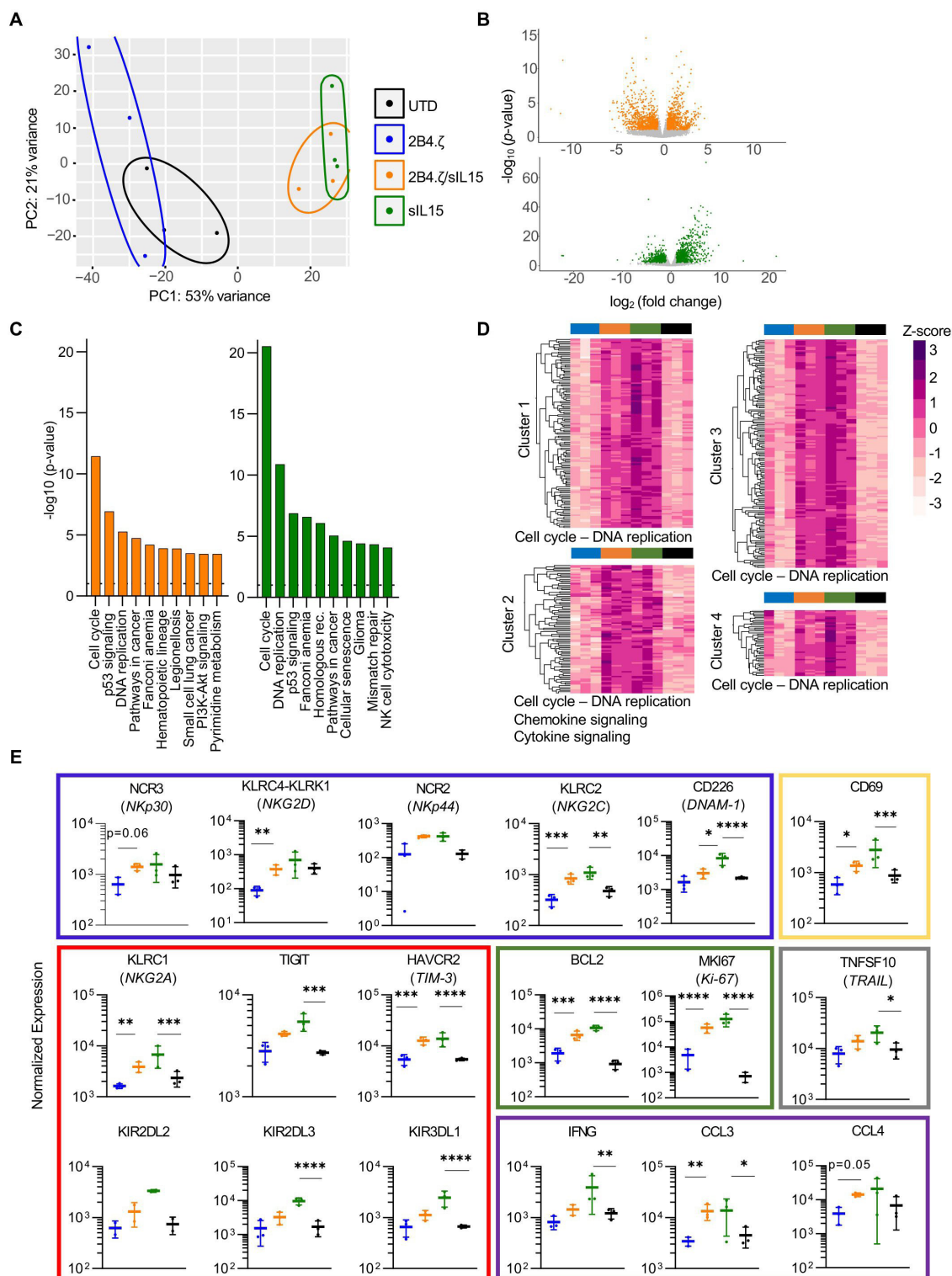
Figure 5 IL-15 stimulation of NK cells upregulates genes important to cell cycle progression, NK-cell activation, and cytotoxicity. (A) PCA of NK-cell transcriptome on D10 of the chronic antigen stimulation. Each dot represents a unique NK-cell donor (n=3 donors). (B) Volcano plots representing differentially regulated genes in 2B4.ζ/sIL-15 compared with 2B4.ζ (orange) and sIL-15 compared with unmodified cells (green). Gray dots are those not meeting criteria: p value ≥0.05; fold change > 2 or <1/2. (C) Bar plot depicting the top 10 significantly different KEGG 2021 human gene set enrichment pathways. Dotted line at a p value of 0.05. (D) Heatmap and hierarchical clustering performed on differentially expressed genes. Biologically relevant clusters and enriched pathways (shown on the bottom of the cluster) represented. Z-score scale bar at right. (E) Dot plots displaying the normalized expression of genes encoding activating receptors (blue rectangle), inhibitory receptors/checkpoint molecules (red), proliferation/antiapoptosis markers (green), inflammatory mediators (purple), death receptor ligands (gray) and activation (yellow) markers (n=3 independent donors). *P<0.05, **P<0.01, ***P<0.001, ****P<0.0001. IL, interleukin; NK, natural killer; PCA, principal component analysis; sIL, secretory interleukin; UTD, untransduced.

survival (days): 2B4.ζ/sIL-15: 25, sIL-15: 21; n=5 mice each group; online supplemental figure 14B). Circulating human IL-15 and NK-cell counts both increased in the 3 weeks from NK-cell injection to death (online supplemental figure 14C,D). Therefore, in our next experiment we decreased our treatment dose of infused NK cells in order to evaluate whether we could mitigate the observed treatment associated mortality. We compared a single decreased dose of 2B4.ζ/sIL-15 CAR-NK cells with multiple doses of 2B4.ζ CAR-NK cells (figure 6A). Infusion of a single dose of 3×10^6 2B4.ζ/sIL-15 CAR-NK and three doses of 3×10^6 2B4.ζ CAR-NK cells both had transient AML control (figure 6B,C). Three doses of 2B4.ζ CAR-NKs prolonged survival, as compared with mice in all other treatment groups (median survival in days; 2B4.ζ vs UTD and untreated; 71 vs 48 and 49, p<0.001; figure 6D). In contrast, even at the lower dose, toxicity and premature death of mice treated with IL-15-secreting NK cells again occurred (median survival in days; 2B4.ζ/sIL-15 vs untreated; 26 vs 49, p<0.001; sIL-15 vs untreated; 21 vs 49, p<0.001; figure 6D). Analysis of PB showed in vivo expansion of 2B4.ζ/sIL-15 and sIL-15 NK cells, with declining NK-cell counts again observed in non-IL-15 secreting NK-cell cohorts (figure 6E). Bone marrow and spleen analysis at necropsy of mice treated with 2B4.ζ/sIL-15 CAR-NKs revealed high numbers of infiltrating NK cells (online supplemental figure 15A,B). We identified increasing systemic hIL-15 in mice treated with 2B4.ζ/sIL-15 and sIL-15 NKs (figure 6F). In addition, high levels of hTNF-α, low levels of mIL-1β and negligible levels of mIL-6 were detected in the blood of mice treated with 2B4.ζ/sIL-15 CAR-NK cells (online supplemental figure 15C–E).

We further evaluated our CAR-NK cells in a more aggressive MOLM-13 xenograft model (figure 6G). A single dose of 3×10^6 2B4.ζ/sIL-15 CAR-NK cells and three doses of 3×10^6 2B4.ζ CAR-NK cells again had equivalent transient antitumor control (figure 6H1). In contrast to the lethal toxicity seen in the MV-4-11 model, both treatment strategies prolonged survival in MOLM-13 engrafted mice (median survival in days: 2B4.ζ vs UTD 26 vs 20, p<0.01; 2B4.ζ/sIL-15 vs UTD 27 vs: 20, p<0.01; figure 6J). Analysis of PB at necropsy showed circulating systemic hIL-15 and hTNF-α, but negligible levels of mIL-1β and mIL-6 (online supplemental figure 16A–D).

DISCUSSION

Herein we describe the generation and functional evaluation of chimeric receptors targeting the AML-associated antigen CD123 and expressed in primary human NK cells. The molecular domains distal to the extracellular scFv consisted of various combinations of NK-specific activation moieties. We identified a 2B4.ζ CAR as having similar in vitro functionality to the well-studied 4-1BB.ζ CAR,[35] with high surface expression, antigen-specific activation, and cytotoxicity. The in vivo antitumor effect was more pronounced when AML-engrafted mice were treated

with 2B4.ζ CAR-NK cells as compared with those treated with 4-1BB.ζ CAR-NK cells, which suggests a potential additive effect of 2B4 and CD3ζ signaling. However, this in vivo effect was short-lived and was accompanied by circulating NK-cell decline. We thus engineered our 2B4.ζ CAR-NK cells with an IL-15 transgene to promote IL-15-mediated activation, proliferation, and survival. Secretion of IL-15 stimulated CAR-NK-cell expansion both in vitro and in vivo, and enhanced short-term and long-term anti-AML cytotoxicity. This bolstered activation profile was confirmed by immunophenotypical and transcriptomic analysis in the setting of chronic stimulation. However, in one in vivo AML model, constitutive IL-15 secretion caused dramatic NK-cell expansion and high levels of circulating human proinflammatory cytokines, and was associated with early death. Treatment with three doses of non-IL-15-secreting CAR-NK cells prolonged survival without systemic toxicity, but antitumor efficacy was transient.

CARs are used to enhance and redirect immune effector cells against cancer cells. CAR-T cells have been extensively investigated in preclinical and clinical models of AML.[9] However, there are limited preclinical animal studies[36 37] and only three active clinical trials (NCT04623944, NCT05008575, and NCT02742727) testing CAR-NK cells as AML therapy. There is a single completed anti-AML CAR-NK-cell trial with evaluable data (NCT02944162). This study tested an engineered anti-CD33 CAR-NK92 cell line in three patients with relapsed and refractory AML. The CD33-CAR NK92 cell infusion was safe, but the treatment had minimal antitumor efficacy.[38] We aimed to enhance the molecular functionality of our CAR by using NK cell-specific receptor domains. We identified the 2B4TM-2B4-CD3ζ CAR as optimal for NK-cell expression and activation. The end result of 2B4 downstream signaling includes synergy with other NK activating receptors.[17 39] Protein interactions including 2B4 occur inside membrane ('lipid') rafts. We chose to use the 2B4 TM domain to localize the CAR within lipid rafts[40] and found that CARs containing a 2B4 TM domain had high surface density and stable CAR expression. Tandem CD3ζ was also important, highlighted by the observed functional differences between 2B4.ζ and 2B4 CAR-NK cells.

To our knowledge, we describe the first study investigating both the in vitro and in vivo anti-AML functionality of peripheral blood-derived CAR-NK cells (PB-NKs) targeting CD123. We chose the PB of healthy donors as the source of our CAR-NK cells. PB-NKs can be isolated through apheresis and expanded in a large scale using feeder cells.[26] PB-NKs are functionally mature, with high activating receptor expression and cytotoxic potency. PB-NKs also display higher levels of KIRs compared with other NK-cell products derived from alternative sources. KIR expression is indicative of more complete NK-cell licensing.[41] Donor-derived, allogeneic PB-NK cells have therapeutic potential due to their relative
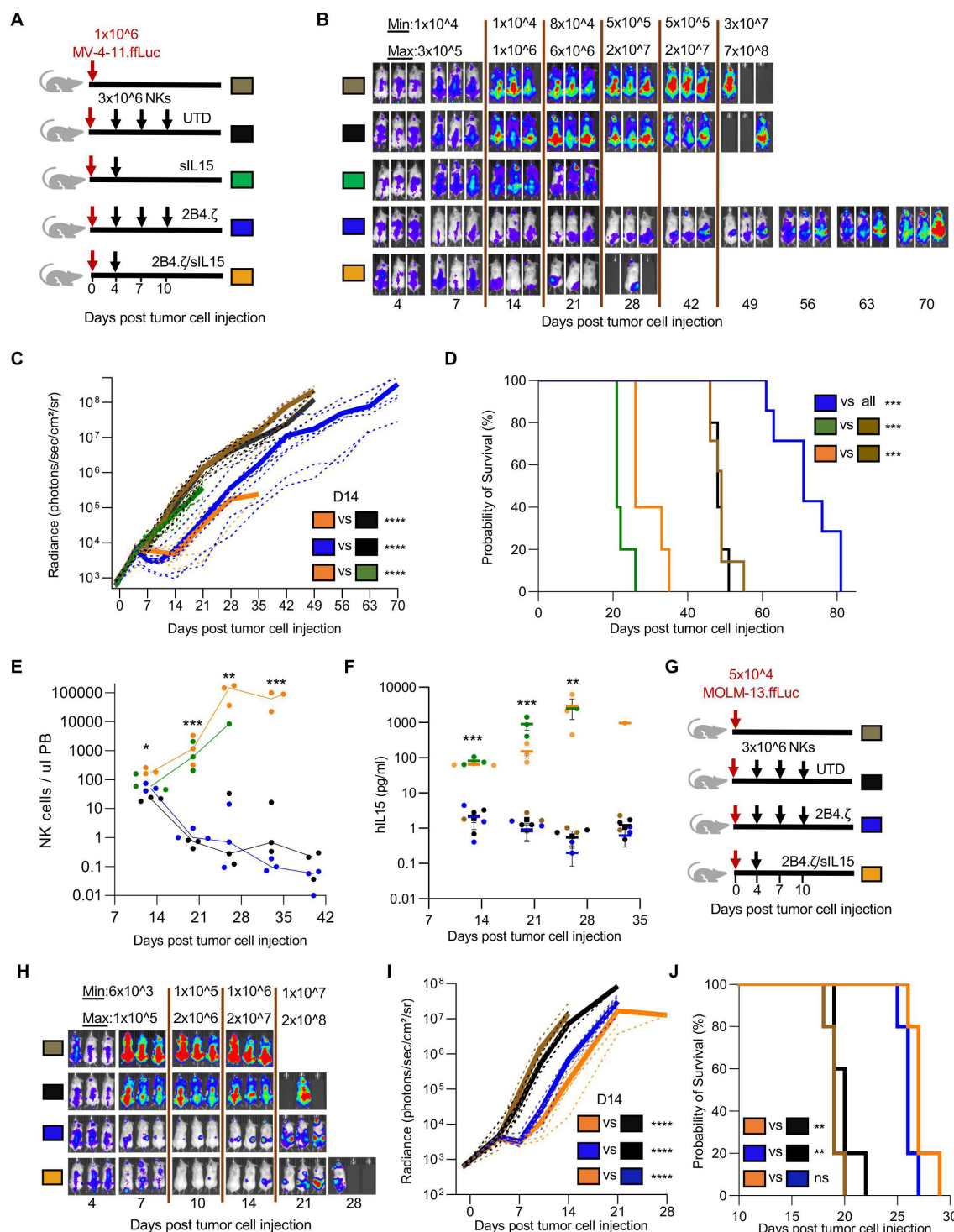
Figure 6 IL-15 secreting CAR-NK cells can cause lethal toxicity in an AML xenograft model. (A) Schematic of NK-cell dosing in MV-4-11.ffLuc model. (B) MV-4-11 proliferation was monitored with BLI. Representative images of mice. The minimum and maximum values of the color scale are indicated (min–max). (C) BL representative of leukemia proliferation was recorded as photons/s/cm²/sr . Dotted lines: individual mice; solid lines: mean (n=5–7 mice per group; two experiments performed for UTD and 2B4.ζ cohorts). (D) Kaplan-Meier survival analysis. (E) Mouse PB was collected at indicated time points and analyzed via flow cytometry. NK-cell numbers per microlitre of mouse PB were tracked starting on D13 of the experiment. Each dot represents cell numbers from a single mouse; line is at median. Asterisks indicate 2B4.ζ/sIL-15 versus 2B4.ζ comparison. (F) Human IL-15 from PB of MV-4-11 engrafted mice drawn at the indicated time points was quantified (pg/mL) with ELISA. Asterisks indicate 2B4.ζ/sIL-15 versus 2B4.ζ comparison. (G) Schematic of NK-cell dosing in MOLM-13.ffLuc model. (H) MOLM-13 proliferation was monitored using BLI (n=5 mice per group). Representative images, (I) radiance, and (J) Kaplan-Meier survival analysis. *P<0.05, **P<0.01, ***P<0.001, ****P<0.0001. AML, acute myelogenous leukemia; BLI, bioluminescence imaging; CAR, chimeric antigen receptor; D, day; ffLuc, firefly luciferase; IL, interleukin; NK, natural killer; PB, peripheral blood; sIL, secretory interleukin; UTD, untransduced.

safety, immediate availability once manufactured and stored, and reduced manufacturing costs as compared with per-patient manufacture of autologous cell therapy products.[12 13] Historically, one challenge facing PB-NK-cell engineering was that of poor viral and non-viral genetic modification.[42] With our method, we are able to achieve high levels of PB-NK transduction. All of our CARs were stably expressed on the surface of primary NK cells, though inter-CAR variability in surface density was observed.

NK cells have a natural life span of approximately 2 weeks in humans. The success of adoptively transferred cellular therapies for cancer is determined, in part, by effector cell persistence. The use of systemic cytokine supplementation is one common strategy employed to support prolongation of NK-cell survival. The short half-life of infused IL-15 necessitates frequent or continuous administration, and systemic toxicity is common.[43–46] IL-15 super agonists, like N-803 (formerly known as ALT-803), have a longer half-life and can mimic physiological IL-15 trans presentation, but administration can cause inflammatory toxicities.[47] The administration of N-803 has been effective at promoting NK-cell proliferation and antitumor efficacy against hematological malignancies, with expected associated fever, chills, and injection site rashes observed.[48–51] Another strategy that has been successful in specifically supporting in vivo CAR-NK-cell survival is engineering constitutive activating cytokine expression.[52] This approach has been shown to be safe in a clinical trial using CD19-CAR NK cells against CD19+ lymphoid malignancies.[53] The demonstrated safety profile motivated us to also test transgenic IL-15 expression with a goal of enhanced in vivo CAR-NK cell persistence. We found NK cells subject to activation with constantly available IL-15 exhibited enhanced and sustained in vitro and in vivo functionality. Though we concluded this to be resultant from specific activation above baseline, it is possible that our NK cells had been rendered 'cytokine addicted'[54] due to ex vivo culture conditions that include supplemental IL-2. In this case, the cohorts of cells without engineered IL-15 secretion may have become dysfunctional once removed from a state of trophic cytokine availability.

In our study, treatment with IL-15 secreting CAR-NK cells caused early death in mice engrafted with MV-4-11 AML. A likely cause of the observed systemic toxicity is severe inflammation due to the dramatic NK-cell proliferation associated with high levels of circulating IL-15 and other proinflammatory cytokines. A CRS-like syndrome triggered by murine monocytes or other immune cells is unlikely due to our inability to detect common murine proinflammatory cytokines. IL-15 stimulation of accelerated leukemic growth was not observed. Clinical signs associated with hyperinflammation (such as weight loss and hunching) are also seen in GVHD and have been observed in our premorbid mice. NK cells have the potential to exacerbate subclinical T cell-mediated acute GVHD.[19] We believe that classically defined GVHD is a less likely cause of our observed toxicity due to the absence of human or murine T cells in our NSG model. However, the possibility of lethal toxicity due to NK-cell alloreactivity against mouse cells cannot be excluded.

We observed that IL-15-secreting CAR-NK cells both prolonged and shortened survival in two xenograft models of AML. Notably, the median survival of mice treated with the same dose of 2B4.ζ/sIL-15 NK cells was similar in each model (MOLM-13: 27 days, MV-4-11: 26 days). This could potentially be explained by the aggressiveness of the MOLM-13 model, as these mice died of widespread disease at roughly the same time as we recorded the onset of treatment-associated mortality. Our observation of unexpected toxicity begs for expanded study of novel ways to stimulate CAR-NK-cell cytokine receptor pathways while circumventing systemic cytokine delivery. Localization of IL-15 with membrane tethering[55] or targeted delivery through the use of oncolytic viruses[56] are alternative therapeutic strategies. Controllable cytokine expression using engineered inducible systems and safety switches also holds promise. Specific activation of intrinsic gamma-cytokine receptor signaling without the use of a pharmacological agent is another strategy that has the potential to sustain NK-cell function with an improved safety profile.

In conclusion, our data underscore the critical nature of IL-15 signaling as a stimulant of CAR-NK-cell long-term survival and anti-AML functionality. Our in vivo data highlight the limitations in murine modeling and the necessity for caution if the use of IL-15 secreting NK cells is planned in human trials of CAR-NK-cell adoptive transfer. Continued therapeutic development is imperative, to include testing of alternate and potentially safer methods of cytokine pathway activation.

REFERENCES

1 Gorman MF, Ji L, Ko RH, *et al*. Outcome for children treated for relapsed or refractory acute myelogenous leukemia (rAML): a therapeutic advances in childhood leukemia (TACL) Consortium study. *Pediatr Blood Cancer* 2010;55:421–9.

2 Döhner H, Estey E, Grimwade D, *et al*. Diagnosis and management of AML in adults: 2017 ELN recommendations from an international expert panel. *Blood* 2017;129:424–47.

3 Yanagisawa B, Perkins B, Karantanos T, *et al*. Expression of putative leukemia stem cell targets in genetically-defined acute myeloid leukemia subtypes. *Leuk Res* 2020;99:106477.

4 Jordan CT, Upchurch D, Szilvassy SJ, *et al*. The interleukin-3 receptor alpha chain is a unique marker for human acute myelogenous leukemia stem cells. *Leukemia* 2000;14:1777–84.

5 Frankel A, Liu J-S, Rizzieri D, *et al*. Phase I clinical study of diphtheria toxin-interleukin 3 fusion protein in patients with acute myeloid leukemia and myelodysplasia. *Leuk Lymphoma* 2008;49:543–53.

6 He SZ, Busfield S, Ritchie DS, *et al*. A phase 1 study of the safety, pharmacokinetics and anti-leukemic activity of the anti-CD123 monoclonal antibody CSL360 in relapsed, refractory or high-risk acute myeloid leukemia. *Leuk Lymphoma* 2015;56:1406–15.

7 Uy GL, Aldoss I, Foster MC, *et al*. Flotetuzumab as salvage immunotherapy for refractory acute myeloid leukemia. *Blood* 2021;137:751–62.

8 Greenbaum U, Mahadeo KM, Kebriaei P, *et al*. Chimeric antigen receptor T-cells in B-acute lymphoblastic leukemia: state of the art and future directions. *Front Oncol* 2020;10:1594.

9 Fiorenza S, Turtle CJ. CAR-T cell therapy for acute myeloid leukemia: preclinical rationale, current clinical progress, and barriers to success. *BioDrugs* 2021;35:281–302.

10 Lee DW, Santomasso BD, Locke FL, *et al*. ASTCT consensus grading for cytokine release syndrome and neurologic toxicity associated with immune effector cells. *Biol Blood Marrow Transplant* 2019;25:625–38.

11 Hines MR, Keenan C, Maron Alfaro G, *et al*. Hemophagocytic lymphohistiocytosis-like toxicity (carHLH) after CD19-specific CAR T-cell therapy. *Br J Haematol* 2021;194:701–7.

12 Köhl U, Arsenieva S, Holzinger A, *et al*. CAR T cells in trials: recent achievements and challenges that remain in the production of modified T cells for clinical applications. *Hum Gene Ther* 2018;29:559–68.

13 Papathanasiou MM, Stamatis C, Lakelin M, *et al*. Autologous CAR T-cell therapies supply chain: challenges and opportunities? *Cancer Gene Ther* 2020;27:799–809.

14 Das RK, Vernau L, Grupp SA, *et al*. Naïve T-cell deficits at diagnosis and after chemotherapy impair cell therapy potential in pediatric cancers. *Cancer Discov* 2019;9:492–9.

15 Ferrara JLM, Levine JE, Reddy P, *et al*. Graft-versus-host disease. *Lancet* 2009;373:1550–61.

16 Chester C, Fritsch K, Kohrt HE. Natural killer cell immunomodulation: targeting activating, inhibitory, and co-stimulatory receptor signaling for cancer immunotherapy. *Front Immunol* 2015;6:601.

17 Lanier LL. Up on the tightrope: natural killer cell activation and inhibition. *Nat Immunol* 2008;9:495–502.

18 Verheyden S, Demanet C. NK cell receptors and their ligands in leukemia. *Leukemia* 2008;22:249–57.

19 Shah NN, Baird K, Delbrook CP, *et al*. Acute GVHD in patients receiving IL-15/4-1BBL activated NK cells following T-cell-depleted stem cell transplantation. *Blood* 2015;125:784–92.

20 Bachiller M, Battram AM, Perez-Amill L, *et al*. Natural killer cells in immunotherapy: are we nearly there? *Cancers* 2020;12 doi:10.3390/cancers12113139

21 Nguyen R, Wu H, Pounds S, *et al*. A phase II clinical trial of adoptive transfer of haploidentical natural killer cells for consolidation therapy of pediatric acute myeloid leukemia. *J Immunother Cancer* 2019;7:81.

22 Shaffer BC, Le Luduec J-B, Forlenza C, *et al*. Phase II study of haploidentical natural killer cell infusion for treatment of relapsed or persistent myeloid malignancies following allogeneic hematopoietic cell transplantation. *Biol Blood Marrow Transplant* 2016;22:705–9.

23 Choi I, Yoon SR, Park S-Y, *et al*. Donor-Derived natural killer cell infusion after human leukocyte Antigen-Haploidentical hematopoietic cell transplantation in patients with refractory acute leukemia. *Biol Blood Marrow Transplant* 2016;22:2065–76.

24 Lee DA, Denman CJ, Rondon G, *et al*. Haploidentical natural killer cells infused before allogeneic stem cell transplantation for myeloid malignancies: a phase I trial. *Biol Blood Marrow Transplant* 2016;22:1290–8.

25 Du X, Ho M, Pastan I. New immunotoxins targeting CD123, a stem cell antigen on acute myeloid leukemia cells. *J Immunother* 2007;30:607–13.

26 Fujisaki H, Kakuda H, Shimasaki N, *et al*. Expansion of highly cytotoxic human natural killer cells for cancer cell therapy. *Cancer Res* 2009;69:4010–7.

27 Nowicka M, Krieg C, Crowell HL, *et al*. CyTOF workflow: differential discovery in high-throughput high-dimensional cytometry datasets. *F1000Res* 2017;6:748.

28 Becht E, McInnes L, Healy J. Dimensionality reduction for visualizing single-cell data using UMAP. *Nat Biotechnol* 2018 doi:10.1038/nbt.4314

29 Van Gassen S, Callebaut B, Van Helden MJ, *et al*. FlowSOM: using self-organizing maps for visualization and interpretation of cytometry data. *Cytometry A* 2015;87:636–45.

30 Love MI, Huber W, Anders S. Moderated estimation of fold change and dispersion for RNA-seq data with DESeq2. *Genome Biol* 2014;15:550.

31 Krawczyk E, Zolov SN, Huang K, *et al*. T-cell activity against AML improved by dual-targeted T cells stimulated through T-cell and IL7 receptors. *Cancer Immunol Res* 2019;7:683–92.

32 Bonifant CL, Szoor A, Torres D, *et al*. CD123-engager T cells as a novel immunotherapeutic for acute myeloid leukemia. *Mol Ther* 2016;24:1615–26.

33 Zolov SN, Rietberg SP, Bonifant CL. Programmed cell death protein 1 activation preferentially inhibits CD28.CAR-T cells. *Cytotherapy* 2018;20:1259–66.

34 Imai C, Mihara K, Andreansky M, *et al*. Chimeric receptors with 4-1BB signaling capacity provoke potent cytotoxicity against acute lymphoblastic leukemia. *Leukemia* 2004;18:676–84.

35 Imai C, Iwamoto S, Campana D. Genetic modification of primary natural killer cells overcomes inhibitory signals and induces specific killing of leukemic cells. *Blood* 2005;106:376–83.

36 Gurney M, Stikvoort A, Nolan E, *et al*. CD38 knockout natural killer cells expressing an affinity optimized CD38 chimeric antigen receptor successfully target acute myeloid leukemia with reduced effector cell fratricide. *Haematologica* 2020 doi:10.3324/haematol.2020.271908

37 Salman H, Pinz KG, Wada M, *et al*. Preclinical targeting of human acute myeloid leukemia using CD4-specific chimeric antigen receptor (CAR) T cells and NK cells. *J Cancer* 2019;10:4408–19.

38 Tang X, Yang L, Li Z, *et al*. First-in-man clinical trial of CAR NK-92 cells: safety test of CD33-CAR NK-92 cells in patients with relapsed and refractory acute myeloid leukemia. *Am J Cancer Res* 2018;8:1083–9.

39 Tangye SG, Cherwinski H, Lanier LL, *et al*. 2B4-mediated activation of human natural killer cells. *Mol Immunol* 2000;37:493–501.

40 Gütgemann SA, Sandusky MM, Wingert S, *et al*. Recruitment of activating NK-cell receptors 2B4 and NKG2D to membrane microdomains in mammalian cells is dependent on their transmembrane regions. *Eur J Immunol* 2015;45:1258–69.

41 Kim S, Poursine-Laurent J, Truscott SM, *et al*. Licensing of natural killer cells by host major histocompatibility complex class I molecules. *Nature* 2005;436:709–13.

42 Boissel L, Betancur M, Lu W, *et al*. Comparison of mRNA and lentiviral based transfection of natural killer cells with chimeric antigen receptors recognizing lymphoid antigens. *Leuk Lymphoma* 2012;53:958–65.

43 Conlon KC, Lugli E, Welles HC, *et al*. Redistribution, hyperproliferation, activation of natural killer cells and CD8 T cells,

and cytokine production during first-in-human clinical trial of recombinant human interleukin-15 in patients with cancer. *J Clin Oncol* 2015;33:74–82.

44 Conlon KC, Potter EL, Pittaluga S, *et al*. Il15 by continuous intravenous infusion to adult patients with solid tumors in a phase I trial induced dramatic NK-cell subset expansion. *Clin Cancer Res* 2019;25:4945–54.

45 Cooley S, He F, Bachanova V, *et al*. First-in-human trial of rhIL-15 and haploidentical natural killer cell therapy for advanced acute myeloid leukemia. *Blood Adv* 2019;3:1970–80.

46 Miller JS, Morishima C, McNeel DG, *et al*. A first-in-human phase I study of subcutaneous outpatient recombinant human IL15 (rhIL15) in adults with advanced solid tumors. *Clin Cancer Res* 2018;24:1525–35.

47 Knudson KM, Hodge JW, Schlom J, *et al*. Rationale for IL-15 superagonists in cancer immunotherapy. *Expert Opin Biol Ther* 2020;20:705–9.

48 Romee R, Cooley S, Berrien-Elliott MM, *et al*. First-in-human phase 1 clinical study of the IL-15 superagonist complex ALT-803 to treat relapse after transplantation. *Blood* 2018;131:2515–27.

49 Rosario M, Liu B, Kong L, *et al*. The IL-15-based ALT-803 complex enhances FcγRIIIa-Triggered NK cell responses and in vivo clearance of B cell lymphomas. *Clin Cancer Res* 2016;22:596–608.

50 Xu W, Jones M, Liu B, *et al*. Efficacy and mechanism-of-action of a novel superagonist interleukin-15: interleukin-15 receptor αSu/Fc fusion complex in syngeneic murine models of multiple myeloma. *Cancer Res* 2013;73:3075–86.

51 Foltz JA, Hess BT, Bachanova V, *et al*. Phase I trial of N-803, an IL15 receptor agonist, with rituximab in patients with indolent non-Hodgkin lymphoma. *Clin Cancer Res* 2021;27:3339–50.

52 Liu E, Tong Y, Dotti G, *et al*. Cord blood NK cells engineered to express IL-15 and a CD19-targeted CAR show long-term persistence and potent antitumor activity. *Leukemia* 2018;32:520–31.

53 Liu E, Marin D, Banerjee P, *et al*. Use of CAR-Transduced natural killer cells in CD19-Positive lymphoid tumors. *N Engl J Med* 2020;382:545–53.

54 Duke RC, Cohen JJ. IL-2 addiction: withdrawal of growth factor activates a suicide program in dependent T cells. *Lymphokine Res* 1986;5:289–99.

55 Imamura M, Shook D, Kamiya T, *et al*. Autonomous growth and increased cytotoxicity of natural killer cells expressing membrane-bound interleukin-15. *Blood* 2014;124:1081–8.

56 Ma R, Lu T, Li Z, *et al*. An oncolytic virus expressing IL15/IL15Rα combined with off-the-shelf EGFR-CAR NK cells targets glioblastoma. *Cancer Res* 2021;81:3635–48.

Supplemental Methods

Cell lines

HEK293T (human embryonic kidney) , Raji (Burkitt's lymphoma) and MV-4-11 (myelomonocytic leukemia) cell lines were purchased from the American Type Culture Collection (ATCC, Manassas, VA) and cultured in Dulbecco's Modified Eagle's Medium (DMEM; ThermoFisher Scientific Waltham, MA; 293T), Roswell Park Memorial Institute (RPMI; ThermoFisher Scientific; Raji) or Iscove's Modified Dulbecco's Medium (IMDM; ThermoFisher Scientific; MV-4-11) supplemented with 10% fetal bovine serum (FBS; HyClone, Logan, UT). MOLM-13 cell line was purchased from the Leibniz Institute (DSMZ, German Collection of Microoganisms and Cell Cultures) and cultured in RPMI supplemented with 10% FBS. CD123 expressing Raji cells (Raji.CD123) were created by first subcloning the full length human CD123 coding sequence into a pCDH lentiviral backbone. Vesicular stomatitis virus G glycoprotein (VSV-G) pseudotyped lentiviral particles were produced using the pPACKH1 HIV Lentivector Packaging Kit (System Biosciences, Palo Alto, CA) according to the manufacturer's instructions and used for Raji cell modification. CD123-positive cells were isolated using fluorescence-activated cell sorting (FACS) and antigen surface expression verified prior to use. All cells used for BLI-based cytotoxicity assays and/or our xenograft models were transduced with a retroviral vector carrying an enhanced green fluorescent protein (GFP) firefly luciferase fusion gene (GFP.ffLuc).[1] GFP-positive cells were sorted and maintained in the appropriate culture medium. Luciferase expression was confirmed using D-luciferin and quantification of bioluminescence. All cells were cultured in a humidified atmosphere containing 5% CO_2 at 37°C.

Determination of Vector Copy Number (VCN)

Primer/probe-FAM was designed to the MMLV-derived psi present in pSFG and purchased from ThermoFisher Scientific. RNAseP primer/probe-VIC/TAMRA mix (Applied Biosystems #4403326) was used as comparison. Genomic DNA was isolated from CAR-NK cells and 25 ng used for amplification with TaqMan Universal PCR Mastermix (ThermoFisher) and the above primer/probe mixes on a C1000 Touch Thermal Cycler (Bio-Rad, Hercules, CA). The following amplification conditions were used: 50°C for 2 minutes, 95°C for 10 minutes, 40 cycles of 95°C for 15 seconds, 60°C for 1 minute. No-template, unmodified NK cells and a condition containing only plasmid were used as controls. Vector copy number calculation was performed using the $2^{-\Delta Ct}$ method.[2]

Cytotoxicity assay

Bioluminescence (BL) based: NK cells were co-cultured with target cells expressing ffLuc at the indicated E:T ratios. D-luciferin was added to plate and BL measured per well. Mean percentage of specific lysis of triplicate samples was calculated as 100*(spontaneous death–experimental death)/(spontaneous death-background). Spontaneous death was measured with control wells containing only target cells. Flow cytometric: NK cells were cultured with target cells. NK and target cell numbers were measured using flow cytometric analysis and NK or target-cell specific markers as above, with dead cell exclusion.

Cytokine secretion assay

100,000 NK cells were plated with an equivalent number of target cells in 0.2 mL media and cultured for 24 hours. Supernatant was collected and IFNγ quantification performed via ELISA (R&D Systems, Minneapolis, MT). For measurement of IL15 secretion, 1 million NK cells were

Supplemental material

BMJ Publishing Group Limited (BMJ) disclaims all liability and responsibility arising from any reliance placed on this supplemental material which has been supplied by the author(s)

J Immunother Cancer

plated in 2 mL media. After 24 hours, supernatant was collected and cytokine quantification was performed with ELISA (R&D Systems) according to the manufacturer's instruction.

Library preparation and RNA sequencing

For RNA sequencing experiments, RNA samples were converted to double stranded cDNA using the Ovation RNA-Seq System v2.0 kit (Tecan, Männedorf, Switzerland), which utilizes a proprietary strand displacement technology for linear amplification of mRNA without rRNA/tRNA depletion as per the manufacturer's recommendations. This approach does not retain strand specific information. Quality and quantity of the resulting cDNA was monitored using the Bioanalyzer High Sensitivity kit (Agilent) which yielded a characteristic smear of cDNA molecules ranging in size from 500 to 2000 nucleotides in length. After shearing 500 nanograms of cDNA to an average size of 250 nucleotides with the Covaris S4 (Covaris Inc., Woburn, MA) library construction was completed with the Truseq Nano kit (Illumina; San Diego, CA) according to the manufacturer's instructions. mRNA libraries were sequenced on an Illumina Novaseq 6000 instrument using 150bp paired-end dual indexed reads and 1% of PhiX control. Reads were aligned to GRCh38 using rsem version 1.3.0 with the following options – star-calc-ci-star-output-genome-bam-forward-prob 0.5.

1. Vera, J.*, et al.* T lymphocytes redirected against the kappa light chain of human immunoglobulin efficiently kill mature B lymphocyte-derived malignant cells. *Blood* **108**, 3890-3897 (2006).

2. Kunz, A.*, et al.* Optimized Assessment of qPCR-Based Vector Copy Numbers as a Safety Parameter for GMP-Grade CAR T Cells and Monitoring of Frequency in Patients. *Mol Ther Methods Clin Dev* **17**, 448-454 (2020).

Supplemental material

BMJ Publishing Group Limited (BMJ) disclaims all liability and responsibility arising from any reliance placed on this supplemental material which has been supplied by the author(s)

J Immunother Cancer

Supplemental Table 1. Detailed list of the fluorophore-conjugated antibodies used in flow cytometry experiments.

Marker	Fluorophore	Clone	Company
CD56	BV421	HCD56	BioLegend
CD56	APC	HCD56	BioLegend
CD56	BUV805	NCAM16.2	BD
CD16	BUV563	3G8	BD
CD33	PerCP/Cyanine5.5	P67.6	BioLegend
CD33	BV785	WM53	BioLegend
His-tag	APC	J095G46	BioLegend
His-tag	PE	J095G46	BioLegend
CD158b (KIR2DL2/2DL3/2DS2)	BUV661	CH-L	BD
CD158e1 (KIR3DL1)	BV480	DX9	BD
CD158 (KIR2DL1/S1/S3/S5)	APC/Fire™ 750	HP-MA4	BioLegend
NKG2A (CD159a)	UV737	131411	BD
NKp30 (CD337, NCR3)	BB700	p30-15	BD
NKp46 (CD335 , NCR1)	BB515	9E2/NKp46	BD
CD57	BV605	QA17A04	BioLegend
CD62L	Red 718	SK11	BD
PVRIG	Alexa Fluor 405	2334A	R&D Systems
TIGIT	BUV395	741182	BD
CD96	BV711	6F9	BD
NKG2D (CD314)	PE-Cy7	1D11	BioLegend
DNAM-1 (CD226)	PE/Dazzle™ 594	11A8	BioLegend
TRAIL (CD253)	BV711	RIK-2	BD
FAS-L (CD178)	BV421	NOK-1	BioLegend
TIM-3 (HAVCR2)	BB700	7D3	BD
LAG3 (CD223)	BV650	11C3C65	BioLegend
PD-1 (CD279)	BB515	EH12.1	BD

Supplemental material

BMJ Publishing Group Limited (BMJ) disclaims all liability and responsibility arising from any reliance placed on this supplemental material which has been supplied by the author(s)

J Immunother Cancer

NKG2C (CD159c)	BV605	134591	BD
2B4 (CD244)	PE-CF594	2-69	BD
KLRG1 (MAFA)	PE-Cy7	2F1/KLRG1	BioLegend
CD69	BUV805	FN50	BD
LFA-1 (CD11a)	Red 718	G-25.2	BD
CD161	BUV395	HP-3G10	BD
TRAIL-R1 (CD261)	BV421	S35-934	BD
FAS (CD95)	BB515	DX2	BD
MICA/MICB (PERB11)	PE-Cy7	6D4	BioLegend
ULBP-1	APC	170818	R&D Systems
CD48	PE-CF594	TÜ145	BD
CD112 (Nectin-2)	PerCP/Cyanine5.5	TX31	BioLegend
CD155 (PVR)	V711	TX24	BD
galectin-9	PE	9M1-3	BD
PD-L1 (CD274)	UV395	MIH1	BD
CD19	PerCP/Cyanine5.5	SJ25C1	BioLegend

Supplemental Table 2. Genes included in the clusters 1-4 shown in Fig. 5D (listed from top to bottom of the cluster).

Cluster 1	Cluster 2	Cluster 3	Cluster 4
RAD54B	CD9	DTL	CTNNA1
MSH5	APOD	CHEK2	ANKRD35
EHHADH	SMOX	CDC45	EFCAB11
SIGLEC7	GPA33	TROAP	RCCD1
HCG27	EGR2	CDKN2C	CDKN2B−AS1
B4GALT6	PAQR4	CCNE1	FAM72B
ZNF90	E2F1	PHF19	C4orf33
SAPCD1	ORC1	MAD2L1	ANXA4
BLVRA	CDT1	WDR76	CD86
MCOLN2	TONSL	IKZF4	SIM1
NEDD4	HIST1H3G	LRP8	TMPO
ACYP1	POLD1	LIN9	FAM72D
ACOT9	HIST1H1B	PTTG1	FBXO43
SORT1	HIST1H2BM	KIF23	CMPK2
CDC42BPA	HAUS8	CCDC150	FN1
KIF18A	HIST1H2AL	EPB41L2	CRTAM
SAPCD1	CENPM	HIST1H1D	KIAA1524
STAP1	NHS	ENTPD1	KPNA2
ANO6	CD84	PHTF2	SGOL2
DBF4	CCNF	RSAD2	CCDC18
LOC100507002	TP73	GEM	ERI2
CENPK	TNC	CASC5	BRCA2
KDELC2	TIAM1	NUF2	CDH17
GBP4	PTPRG	UBE2T	MELK
GGCT	GOLGA8G	FANCI	CDC7
SIRPG	ADGRL2	RAD51AP1	RRM2
BARD1	ZFHX3	NUSAP1	HJURP
GZMA	WNT7B	POLQ	DIAPH3
DGKA	DRAXIN	NCAPH	SHCBP1
FBXO44	GOLGA8DP	CLSPN	KNTC1
CENPQ	BCL2L11	UBE2C	E2F8
ARL6IP6	GOLGA8F	STMN1	KIF20A
NEIL3	FRMD5	FOXM1	DEPDC1B
ELOVL6	ACVR1B	SKA1	TMPO
CENPE	CHRM3−AS2	TYMS	TACC3
CCNE2	ADAM19	C2orf48	DDIAS
DPP4	NCR2	CDC25C	KIF15
HTATSF1	VWA2	SPC25	TTK

Supplemental material

BMJ Publishing Group Limited (BMJ) disclaims all liability and responsibility arising from any reliance placed on this supplemental material which has been supplied by the author(s)

J Immunother Cancer

FBXO5	DYSF	GINS2	E2F7
YEATS4	RGS16	LOC81691	CEP55
SMC4	FAM221A	MAL	NEK2
STARD4	CCL3L3	EME1	ACAT2
CCNG1	MIR210HG	BRCA1	OAS3
KIR2DL4	CCL4	XRCC2	INCENP
TNS4	CCL3	SGOL1	
MYBL1	HIST2H2AB	CCDC34	
GPR171	HAPLN3	PTGIS	
KIF20B	TNFSF12	PTPN3	
SYCP2	OMD	ASF1B	
DCK	PSMC3IP	PKMYT1	
NTRK2	HACD1	MYBL2	
DMRT2	SDC4	E2F2	
NEDD9	DTYMK	RAD54L	
CEP152	LRRC20	EDA2R	
ARHGAP11A	SMCO4	LOC100506985	
PDGFRB	PRADC1	RCAN3	
SOCS2	LTA	HIST1H3B	
ARNTL2	FAAP24	MCM4	
ERI1	FANCC	SPAG5	
IFI44	CENPH	GINS3	
EZH2	C17orf53	ORC6	
GBP1	TK1	SAPCD2	
OPHN1	LOC642846	CKS1B	
LOC100288637	UNQ6494	TUBA1B	
FBXO2	TNFRSF8	TUBB	
AFAP1L2	C16orf59	HIST1H2BH	
LTB	TRAIP	RMI2	
PIF1	FBXO6	CCNB1	
LAIR2	FANCG	EXO1	
EPDR1	DMD	CDC6	
HOXB6	IFI27L1	BUB1B	
CD80	AURKB	CENPI	
NUGGC	STXBP5L	GTSE1	
RNASE4	DMC1	TICRR	
CHEK1	OIP5	IQGAP3	
CDKN3	MCOLN3	DLGAP5	
CREM	APOBEC3B	CIT	
KIF11	KIF4A	AURKA	
PLK4	KIF24	BCL2	

Supplemental material

BMJ Publishing Group Limited (BMJ) disclaims all liability and responsibility arising from any reliance
placed on this supplemental material which has been supplied by the author(s)

J Immunother Cancer

RBBP8	TMEM106C	ASPM	
HMGB2	NRM	STIL	
DNAJC9	CENPN	PRIM1	
FAM72C	CENPP	CDK1	
PRTFDC1	CDK2	TPX2	
LEF1	UBASH3B	ANLN	
TNFSF8		PRR11	
FAS		CDCA2	
ATAD2		PRC1	
CENPU		MKI67	
RRM1		ESCO2	
TCF19		TOP2A	
BRIP1		KIF14	
DEPDC1		HMMR	
CKAP2L		CCNB2	
NCAPG		CDCA3	
ECT2		CDCA8	
NDC80		KIF18B	
ZNF367		MCM10	
RGS6		CDC20	
TJP1		KIFC1	
ITGA2		TIMELESS	
CEACAM1		KIF2C	
HOXB7		KIAA0101	
MB21D2		ZWINT	
SLAMF1		WDR62	
LOC100294145		CDCA5	
FANCD2		PLK1	
RNF157		RAD51	
C1orf112		CDC25A	
MASTL		DSN1	
MBOAT2		SUV39H1	
POLE2		POC1A	
C18orf54		CBR3	
LOC399815		FDXR	
ZNF730		LIG1	
TEX30		BIRC5	
USP18		ESPL1	
HMSD		UHRF1	
LINC00892		CENPW	
SERPINE2		PCNA	

Supplemental material

BMJ Publishing Group Limited (BMJ) disclaims all liability and responsibility arising from any reliance placed on this supplemental material which has been supplied by the author(s)

J Immunother Cancer

ACTA2		CENPA	
TSPAN5		WDHD1	
B4GALNT1		TRIP13	
LINC00504		DHFR	
NDFIP2		FAM111B	
NCAM1		SKA3	
		SMC2	
		CCNA2	
		GGH	
		STX3	
		RACGAP1	
		DSCC1	
		RBL1	
		ANXA9	
		APOL4	
		C21orf58	
		GINS4	
		MCM2	
		HIRIP3	
		MCM3	
		MTFR2	
		GINS1	
		NCAPG2	
		CHAF1B	
		RPL39L	
		NPC2	
		IFNLR1	
		OAS1	
		CKS2	
		GMNN	
		KDELC1	
		ARHGAP11B	

Supplemental material

BMJ Publishing Group Limited (BMJ) disclaims all liability and responsibility arising from any reliance placed on this supplemental material which has been supplied by the author(s)
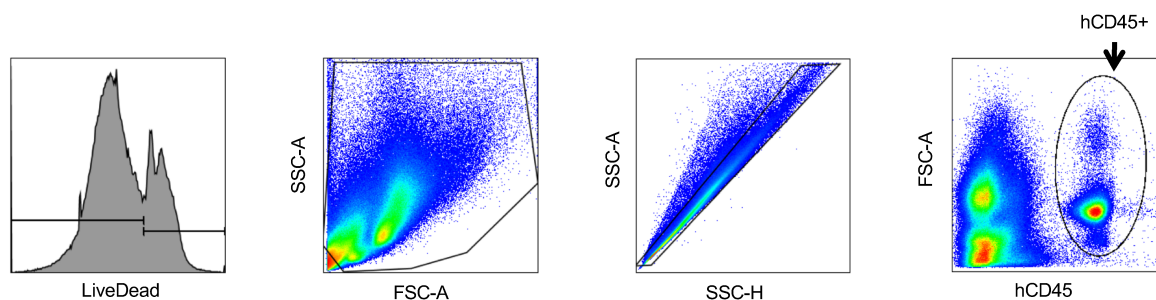
J Immunother Cancer

A.

B.

C.
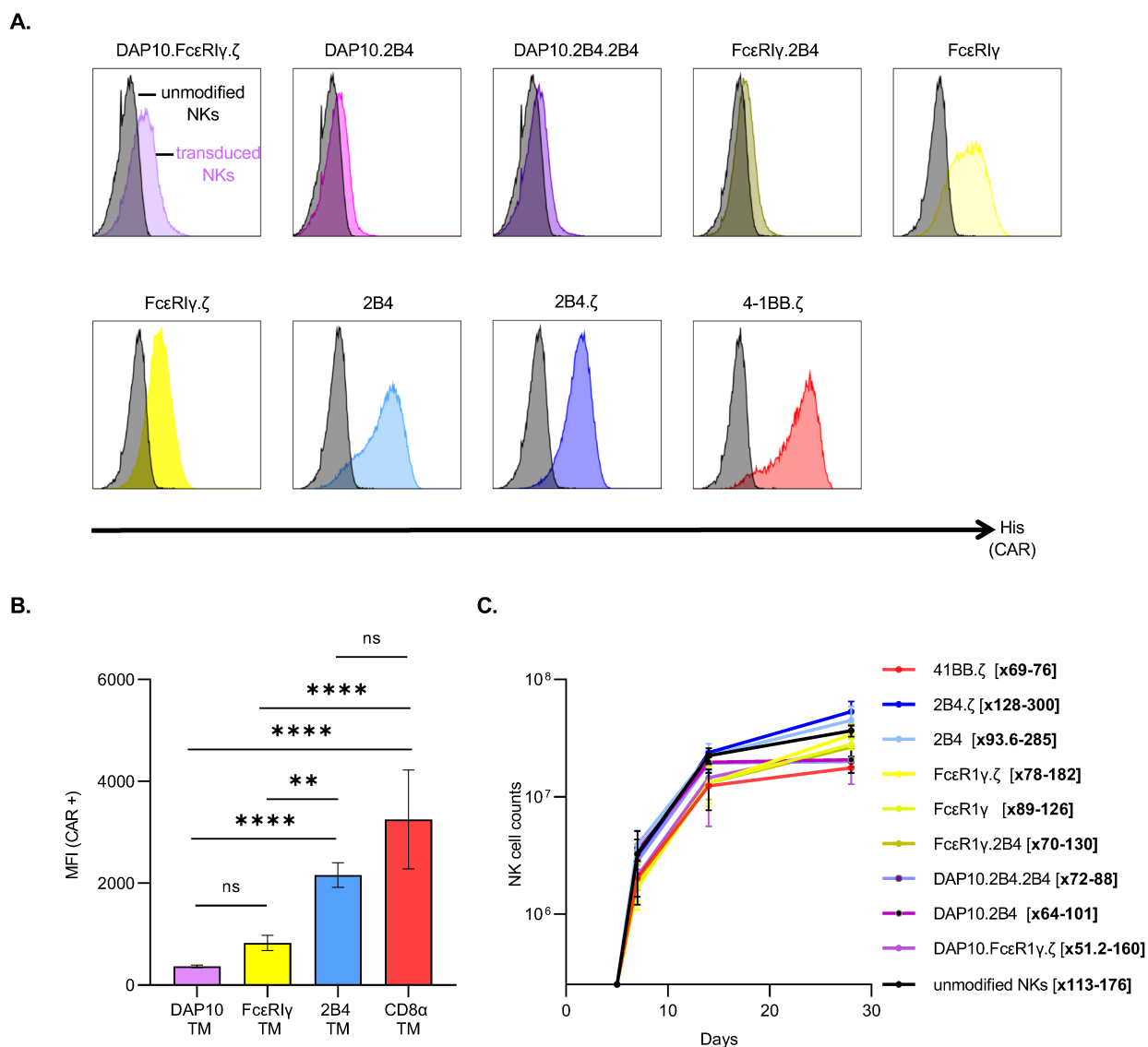
Supplemental Figure 1. CAR expression and proliferative rate of CAR-NK cells. (**A**) FACS plots representing the gating strategy used to identify CAR+ NK cells. (**B**) Bar plot comparing the mean fluorescence intensities +/- SEM of CARs with indicated transmembrane (TM) domains. (**C**) Rate of expansion of our CAR-NK cells calculated with manual counting of absolute number. Initial seeding count was 250,000 cells. Fold expansion indicated in [ ] to the right of legend. Mean +/- SEM (n=3 donors).
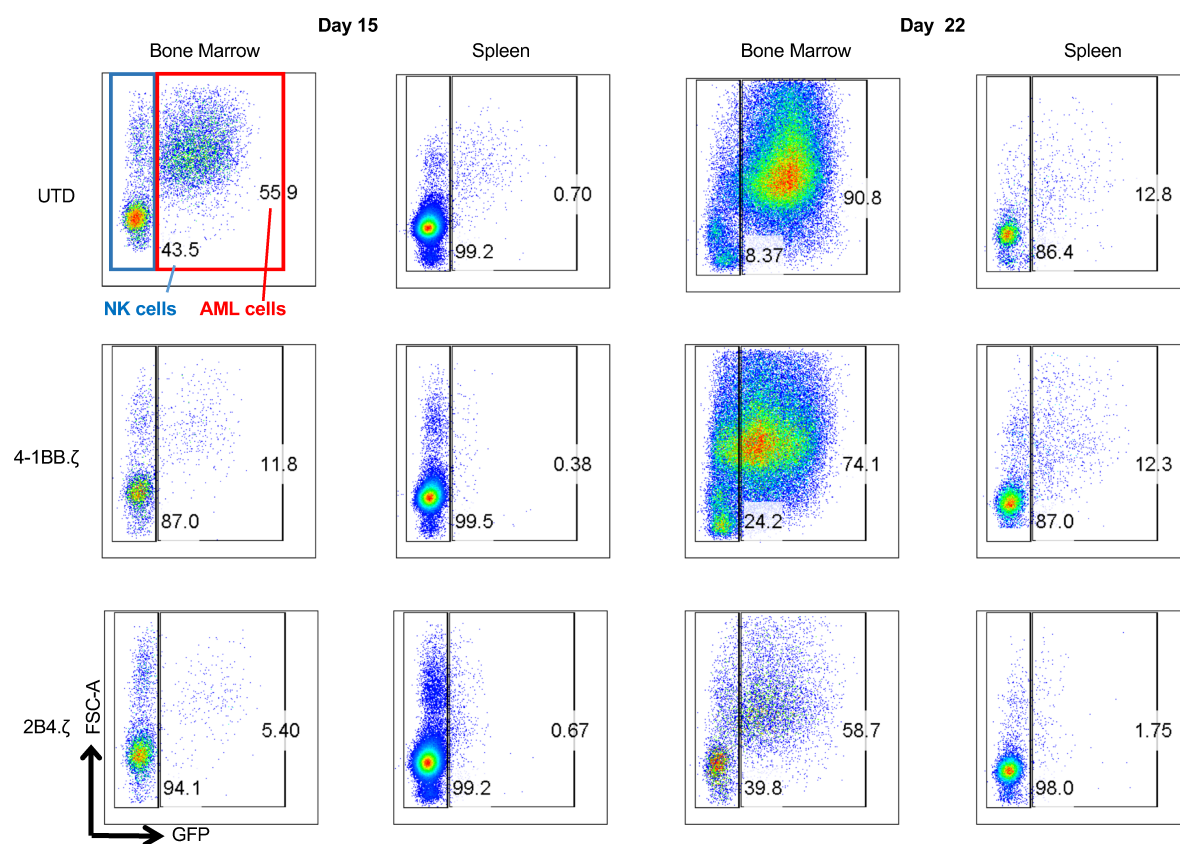
Supplemental material

BMJ Publishing Group Limited (BMJ) disclaims all liability and responsibility arising from any reliance placed on this supplemental material which has been supplied by the author(s)

J Immunother Cancer
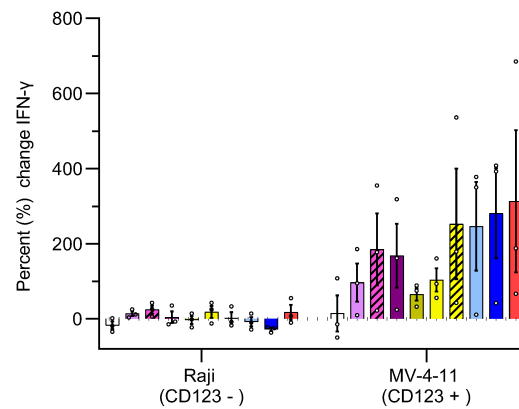
Supplemental Figure 2. Anti-CD123 CAR-NK cells are activated by CD123+ cells. Percent (%) change of IFNγ secretion from baseline measured at 24-hours in co-culture assays of indicated CAR-NKs with Raji [CD123(-)] and MV-4-11 [CD123 (+)] cancer cell lines. IFNγ secretion was measured with ELISA. Each bar representative of the mean plus or minus the standard error of mean (+/- SEM); each dot is representative of an individual NK cell donor.

Supplemental material

BMJ Publishing Group Limited (BMJ) disclaims all liability and responsibility arising from any reliance placed on this supplemental material which has been supplied by the author(s)

J Immunother Cancer

Supplemental Figure 3. NK and leukemia cell percentages in the bone marrow and spleen of MV-4-11 engrafted mice on experimental days 15 and 22. A. Gating strategy used to identify hCD45+ cells in all *in vivo* experiments. LiveDead negative cells (alive) → excluding cellular debris → Single cells→ human CD45 positive (+) cells (human cells). **B.** FACS plots of hCD45(+) cells in the bone marrow and spleen of mice on day 15 (8 days after NK cell injection) and on day 22 (15 days after NK cell injection). MV-4-11.ffLuc cells (red rectangle) are GFP positive. Numbers represent percentages of NK or AML cells. One mouse analyzed per condition per day.

A.

B.
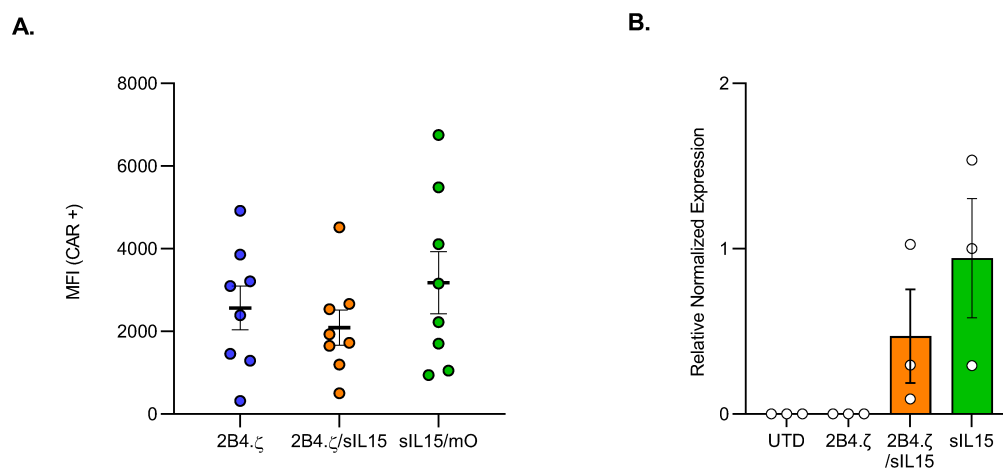
Supplemental Figure 4. Expression of CARs and IL15 in NK cells. (**A**) Mean fluorescence intensity (MFI) of CAR (2B4.ζ and 2B4.ζ/sIL15) or mOrange (sIL15/mO) expression on transduced NK cells (n=4 donors measured at 2 time points). (**B**) Transgenic IL15 expression measured with Real-Time quantitative PCR. Normalized gene expression plotted relative to donor #3 sIL15 condition. GAPDH used as reference gene for normalization of gene expression (n=3 donors).
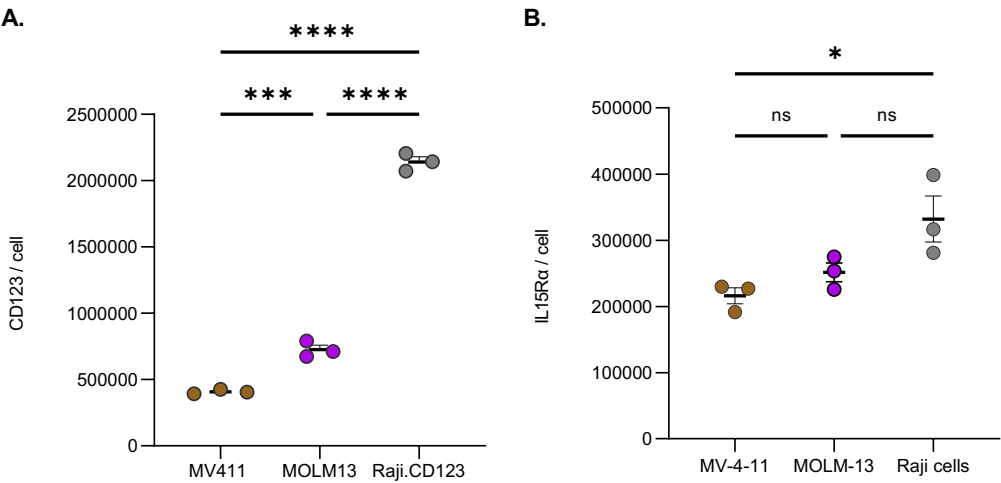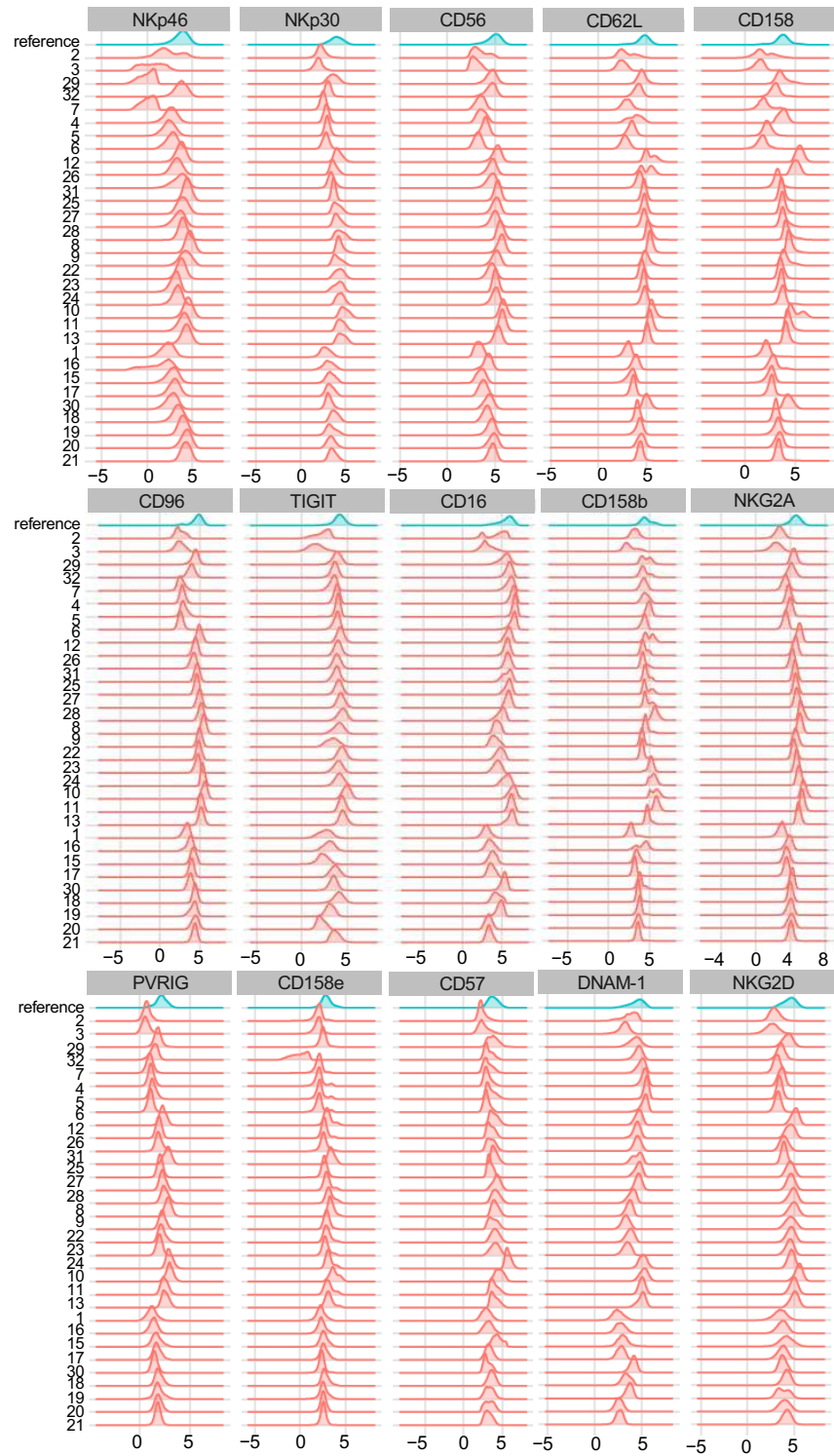
Supplemental Figure 5. Surface antigen quantification on target cells. Quantification of (**A**) CD123 and (**B**) IL15Rα per cell (*p<0.05; ***p<0.001; ****p<0.0001).
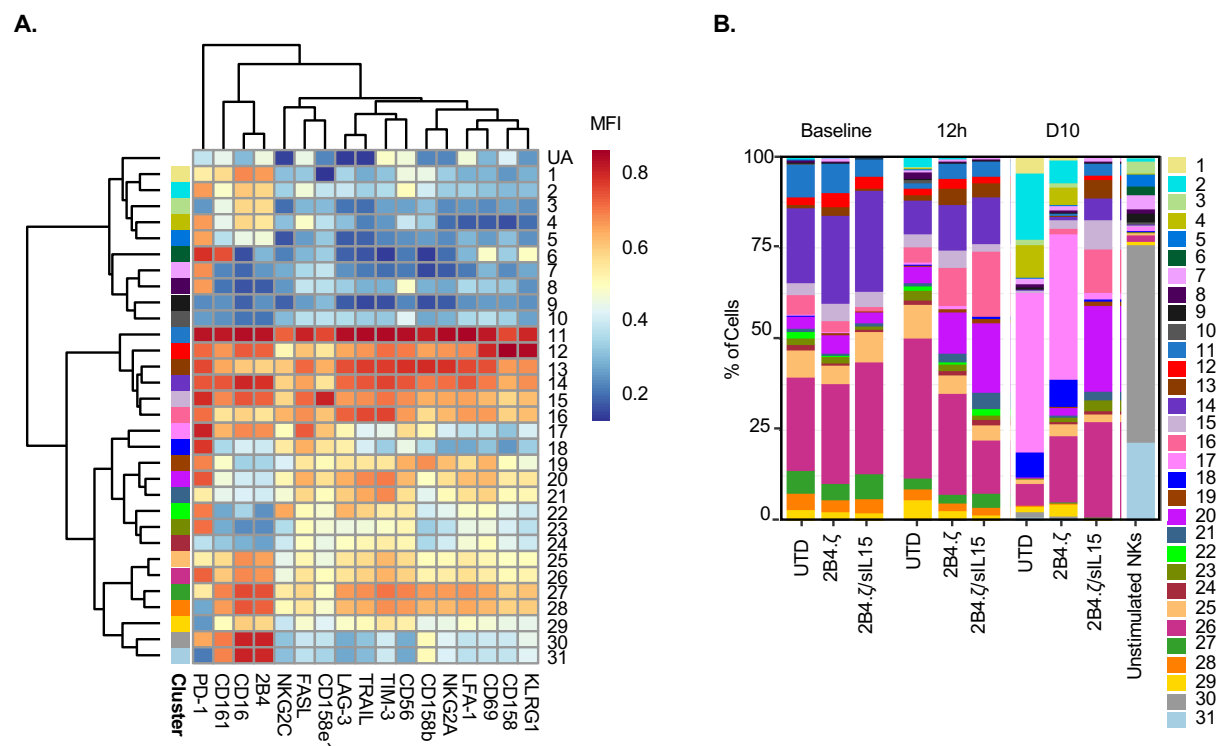
Supplemental Figure 6. IL15-secreting CAR-NK cells demonstrate a distinct phenotype after chronic antigen stimulation. (**A**) Heatmap of flow cytometry data showing expression of 17 different NK cell surface markers. Heatmap coloring represents arcsinh transformed median marker intensities. (**B**) Bar plots of relative abundance of the 31 population subsets found in each sample. *The population clusters of the first panel (shown in **Fig. 4**) are not the same (numbers/colors) as the ones of the second panel, shown here.* Unstimulated, freshly isolated NK cells are used as controls.

Supplemental material

BMJ Publishing Group Limited (BMJ) disclaims all liability and responsibility arising from any reliance placed on this supplemental material which has been supplied by the author(s)

J Immunother Cancer

Supplemental Figure 7. Distribution of marker intensities of indicated "Panel A" receptors in the identified 32 NK cell clusters. The NK cell clusters (on the left side) are named as in **Figure 4**. Red histograms represent the respective marker in each cluster. Blue histograms are a reference calculated from all cells.
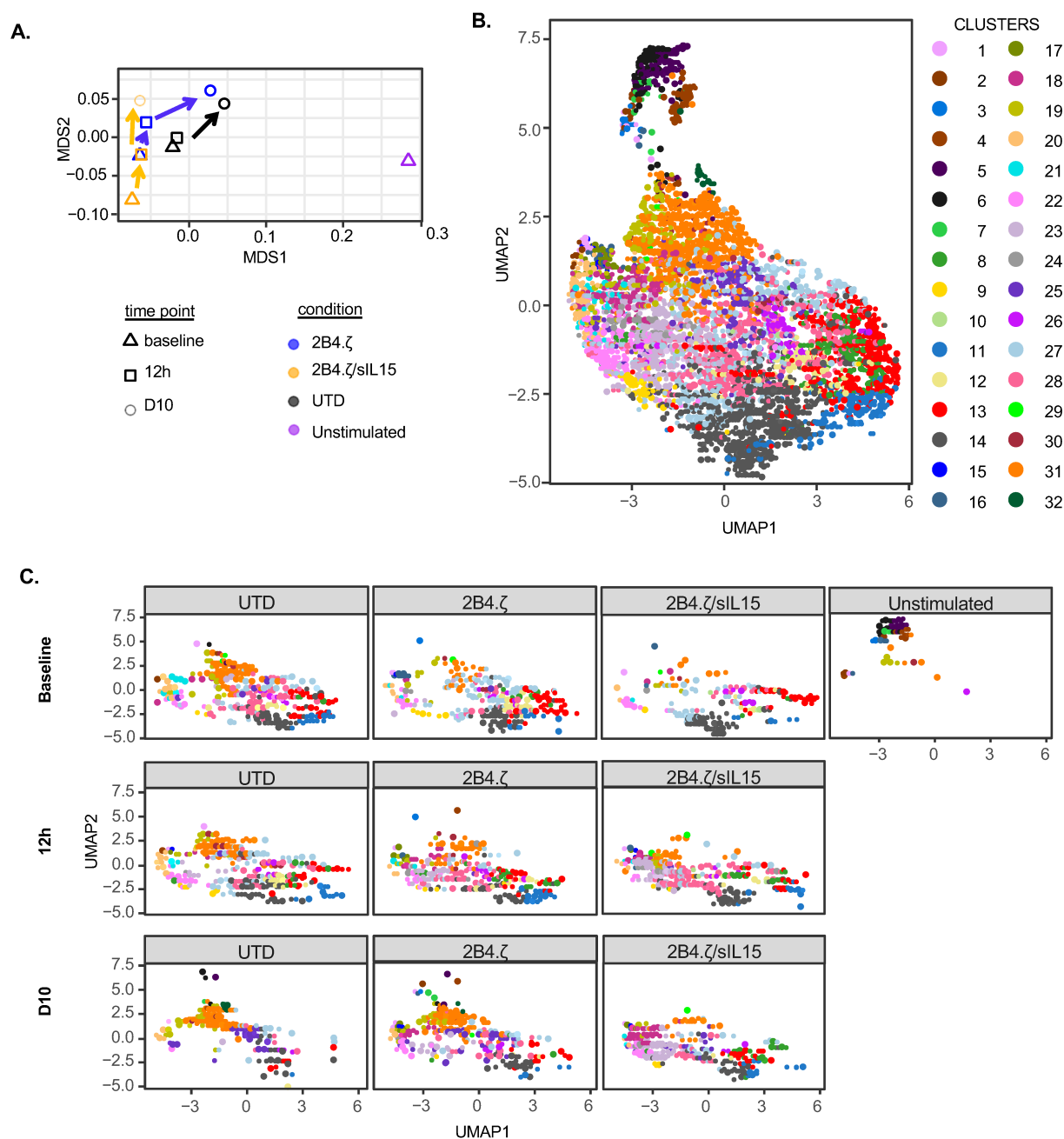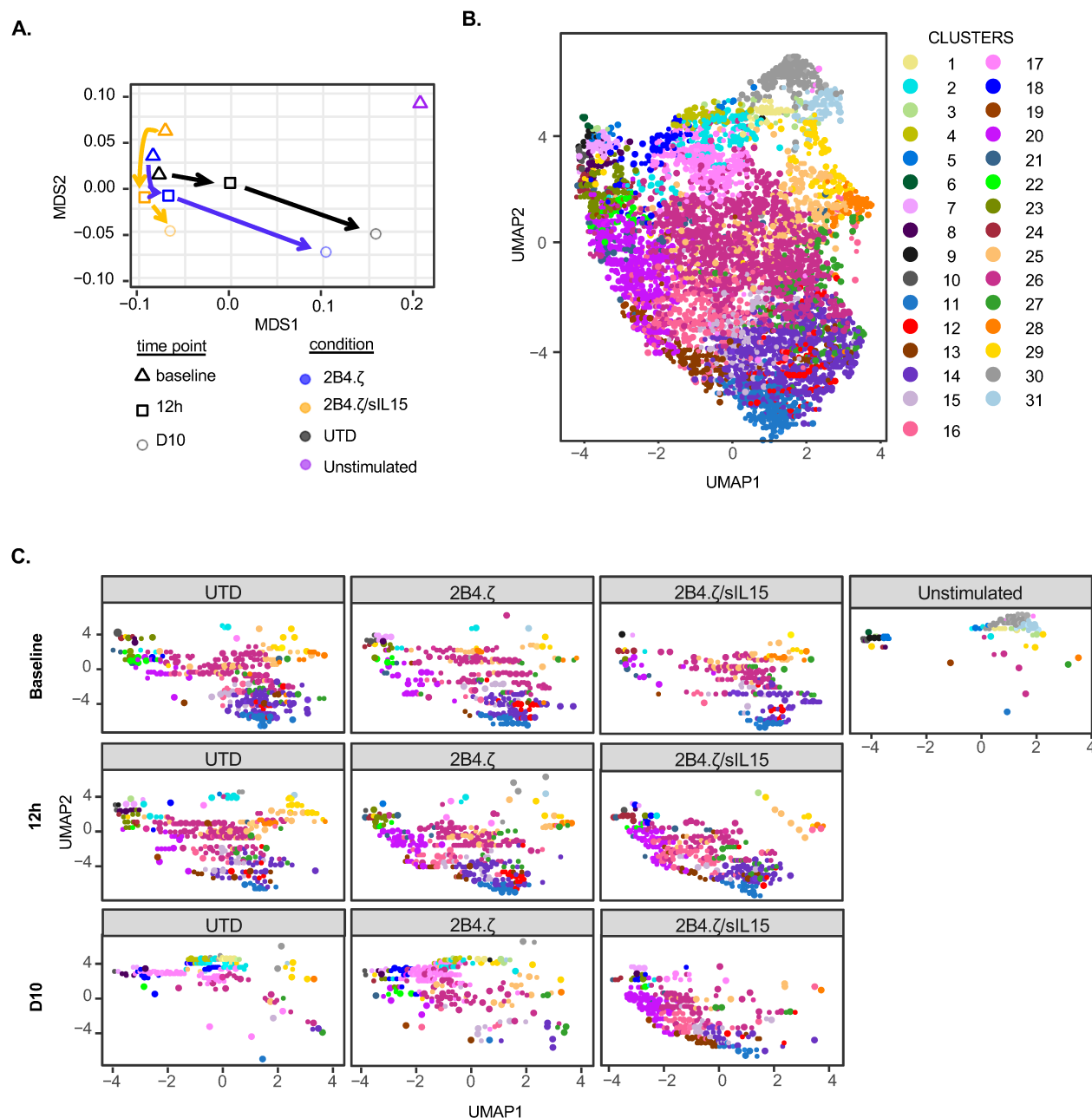
Supplemental Figure 8. Visual representation of "Panel A" immunophenotype data (**A**) Multidimensional scaling (MDS) plot. Unstimulated, freshly isolated NK cells are used as controls. Arrows indicate the transitions across timepoints of experiment. (**B**) Uniform Manifold Approximation and Projection (UMAP) plot was generated based on the arcsinh-transformed expression of the 15 expression markers in the NK cells from the whole dataset. Cells are colored according to the 32 clusters generated after manually merging the 40 meta-clusters obtained with FlowSOM. (**C**) Individual UMAP plots of different NK cell conditions. Different time points indicated on the left side (baseline, 12h, D10).
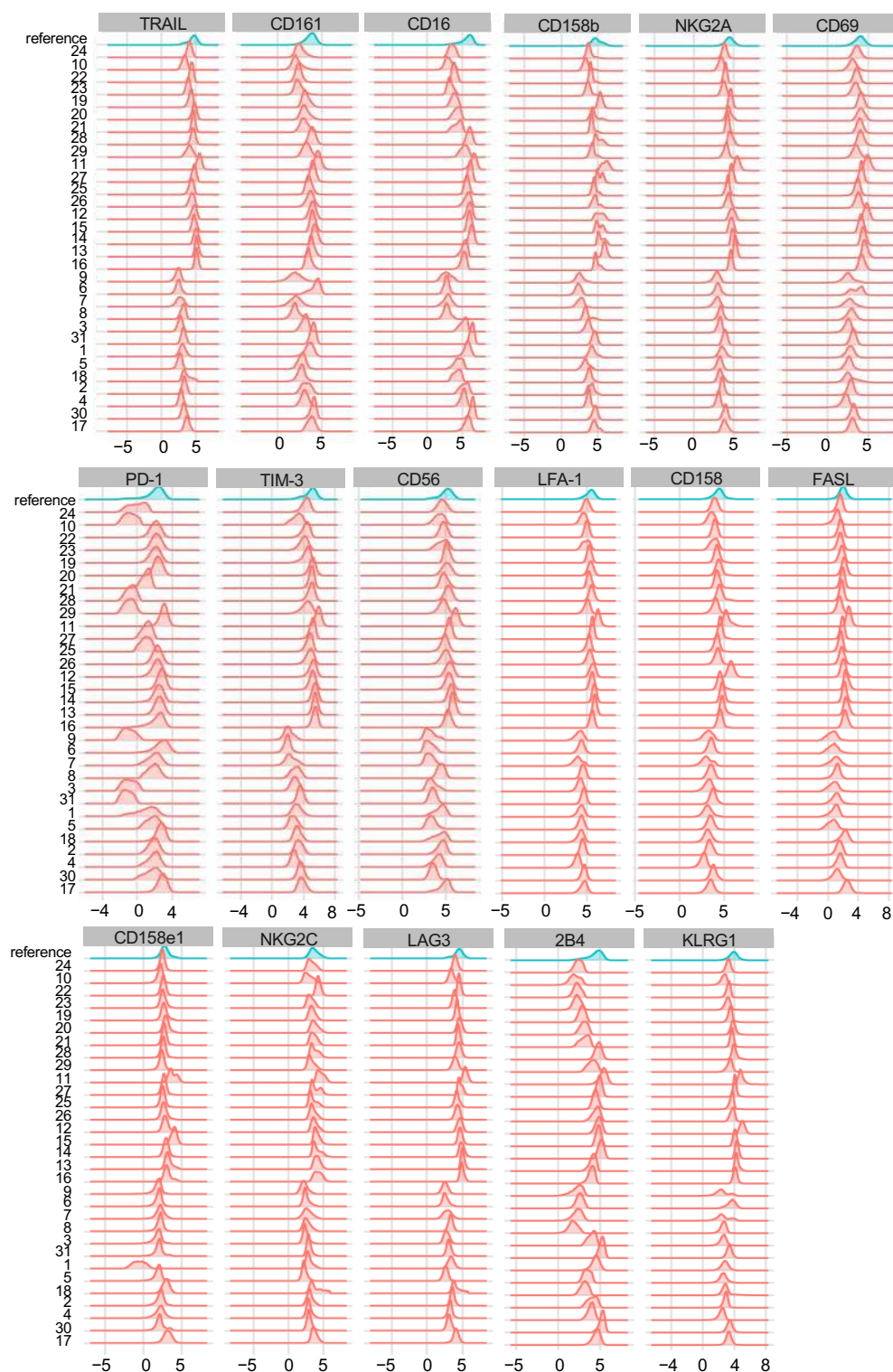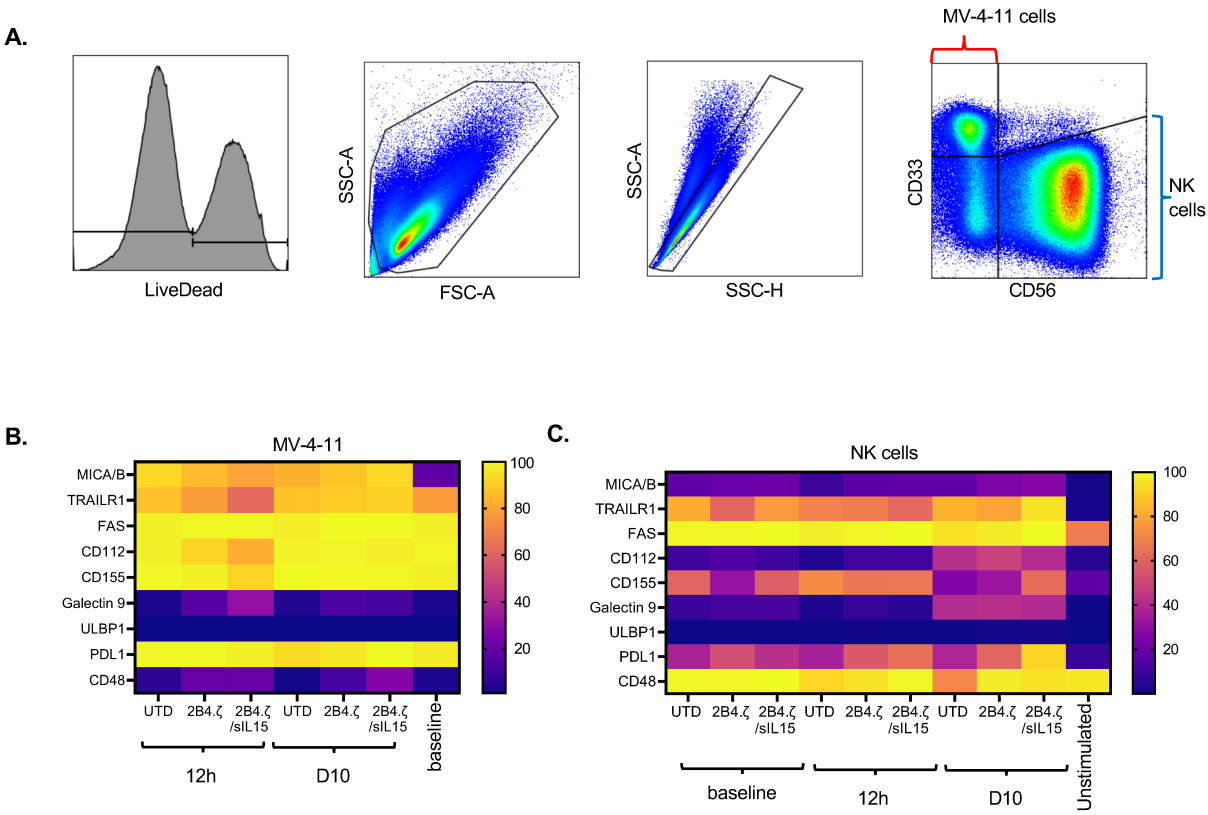
Supplemental Figure 9. Distribution of marker intensities of the indicated "Panel B" receptors in the 31 NK cell clusters. The NK cell clusters (on the left side) are specific for **Supplemental Fig. 6.** Red histograms represent the respective marker in each cluster. Blue histograms are a reference calculated from all cells.
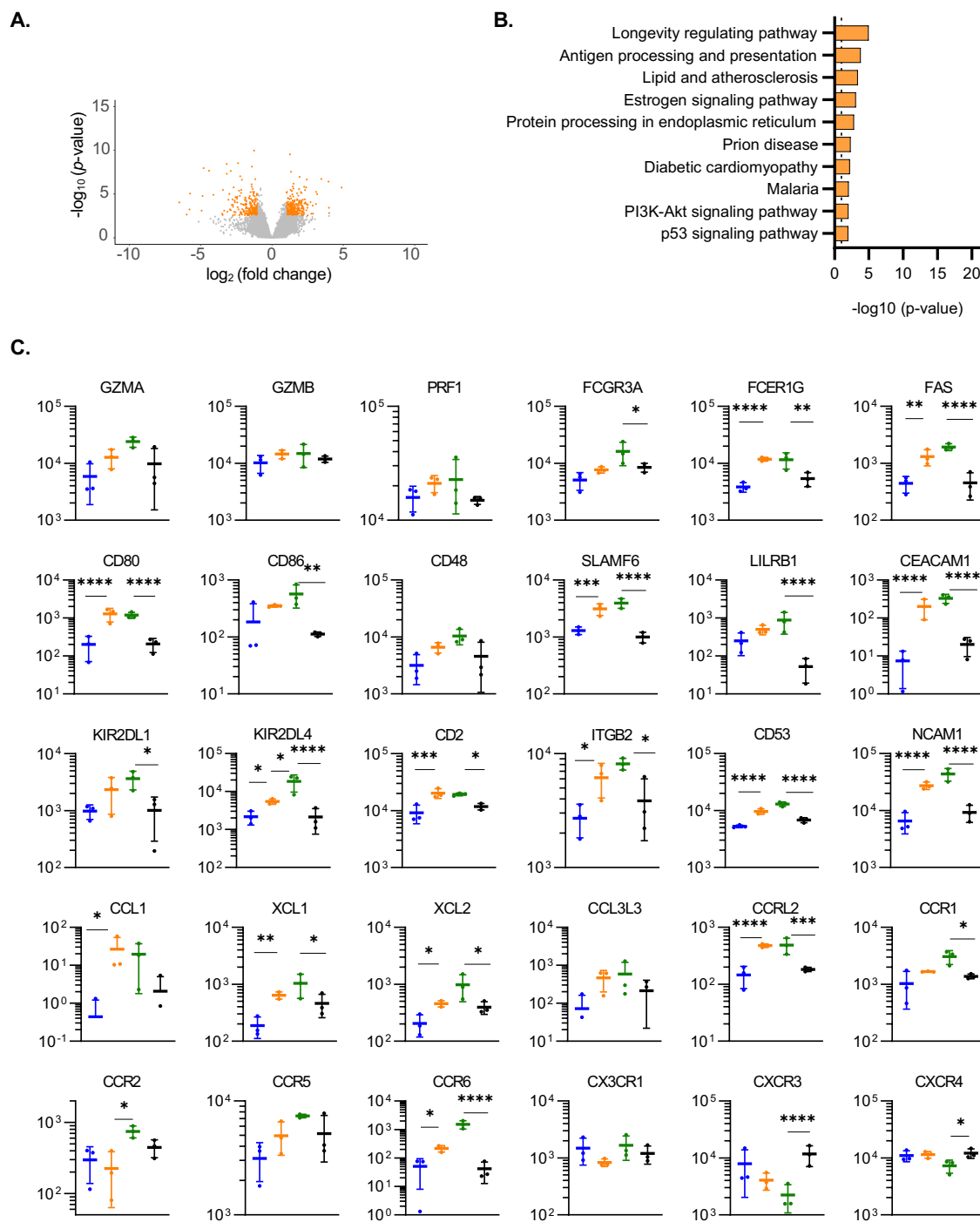
Supplemental material

BMJ Publishing Group Limited (BMJ) disclaims all liability and responsibility arising from any reliance placed on this supplemental material which has been supplied by the author(s)

J Immunother Cancer

Supplemental Figure 10. Visual representation of "Panel B" immunophenotype data (**A**) Multidimensional scaling (MDS) plot. Unstimulated, freshly isolated NK cells are used as controls. Arrows indicate the transitions across timepoints of experiment. (**B**) Uniform Manifold Approximation and Projection (UMAP) plot was generated based on the arcsinh-transformed expression of the 17 expression markers in the NK cells from the whole dataset. Cells are colored according to the 31 clusters generated after manually merging the 40 meta-clusters obtained with FlowSOM. (**C**) Individual UMAP plots of different NK cell conditions. Different time points indicated on the left side (baseline, 12h, D10).

Supplemental material

BMJ Publishing Group Limited (BMJ) disclaims all liability and responsibility arising from any reliance placed on this supplemental material which has been supplied by the author(s)

J Immunother Cancer

Supplemental Figure 11. Expression of NK cell receptor ligands on target and NK cells. (**A**) Gating strategy. (**B**) Heatmap of the percent (%) expression of indicated ligands on MV-4-11 cells or (**C**) NK cells at each experimental time point.

Day-block legend (upper left corner of each cell):

D1	D2	D3
D4	D5	D6
D7	D8	D9
D10		

	2B4.ζ			sIL15			2B4.ζ /sIL15		
UTD	< 0.0001	<0.0001	<0.0001	< 0.0001	< 0.0001	< 0.0001	< 0.0001	< 0.0001	< 0.0001
	0.053	>0.99	>0.99	< 0.0001	< 0.0001	< 0.0001	< 0.0001	< 0.0001	< 0.0001
	>0.99	>0.99	>0.99	0.0002	0.0023	0.98	< 0.0001	< 0.0001	< 0.0001
	>0.99			>0.99			0.0016		
2B4.ζ				>0.99	0.0054	< 0.0001	>0.99	0.0024	< 0.0001
				< 0.0001	< 0.0001	< 0.0001	< 0.0001	< 0.0001	< 0.0001
				< 0.0001	0.0023	0.98	< 0.0001	< 0.0001	< 0.0001
				>0.99			0.0016		
sIL15							>0.99	>0.99	>0.99
							0.504	0.846	0.032
							< 0.0001	< 0.0001	< 0.0001
							0.0016		

Supplemental Figure 12. Comparisons of mean percent (%) cytotoxicity between different NK cell conditions in the serial stimulation assay shown in Fig. 4E. Each cell is subdivided to represent days 1-10 as indicated in upper left corner. Every cell's value signifies the p-value of each comparison for every day. P values generated with ordinary 2-way ANOVA corrected for multiple comparisons using the method of Bonferroni.
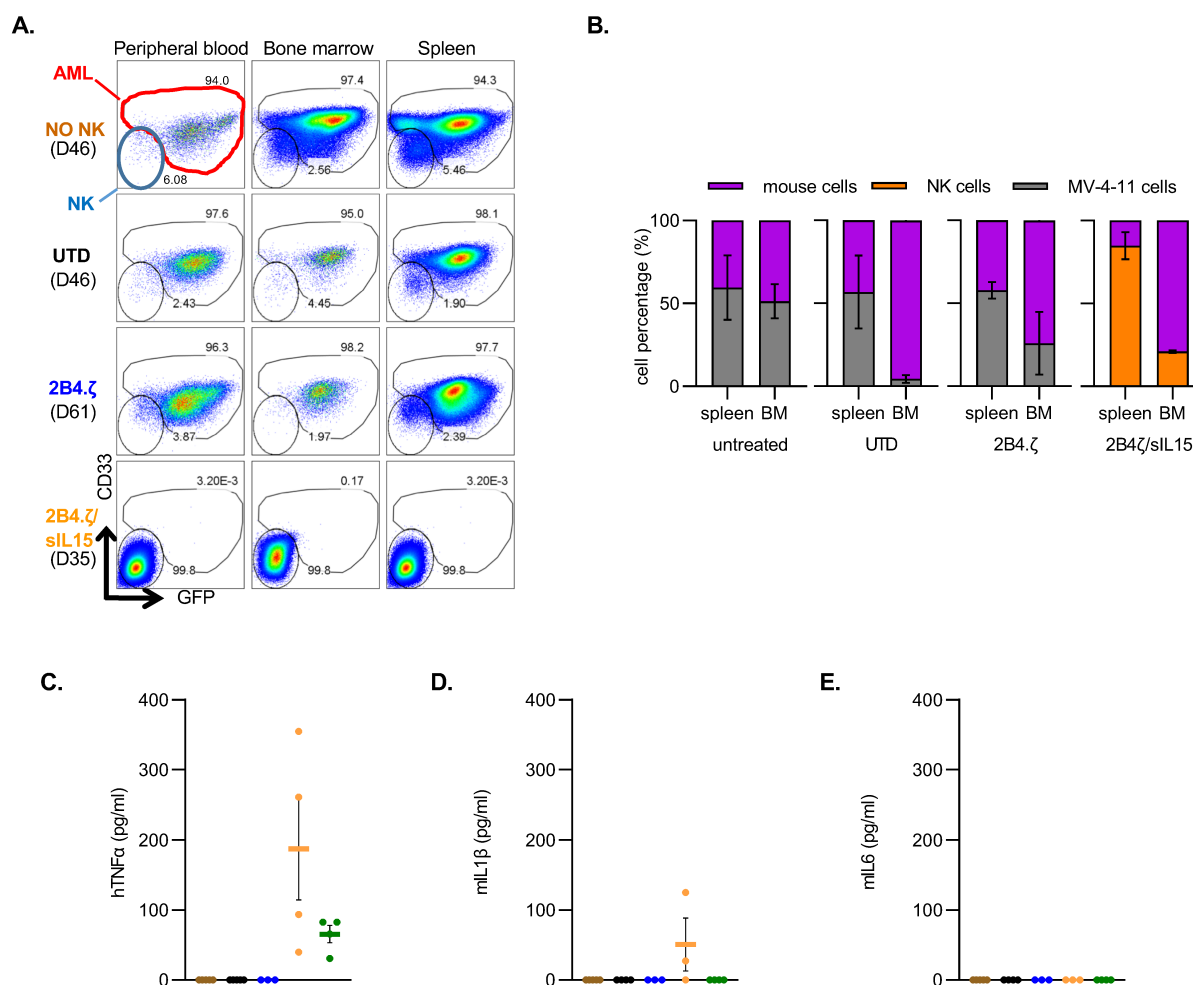
Supplemental material

BMJ Publishing Group Limited (BMJ) disclaims all liability and responsibility arising from any reliance placed on this supplemental material which has been supplied by the author(s)

J Immunother Cancer

Supplemental Figure 13. Transcriptomic evaluation of individual genes and differential expression analysis of IL15 secreting NKs. (**A**) Volcano plot representing upregulated and downregulated genes in 2B4.ζ/sIL15 compared to sIL15 NK cells. Orange dots on the left represent downregulated and dots on the right represent upregulated genes. Location of each data point is calculated as log2(FC) × −log10(p-value). Color cutoffs: p-value < 0.05; fold change cutoff >2 or <1/2. (**B**) Bar plot depicting the top 10 significant pathways enriched in the differentially expressed genes. KEGG 2021 Human gene Set Enrichment Analysis was used. Dotted line represents the cutoff p-value of 0.05.(**C**) Dot plots displaying the normalized expression of individual genes (n=3 independent donors). Statistical significance: *p<0.05; **p<0.01; ***p<0.001; ****p<0.0001.
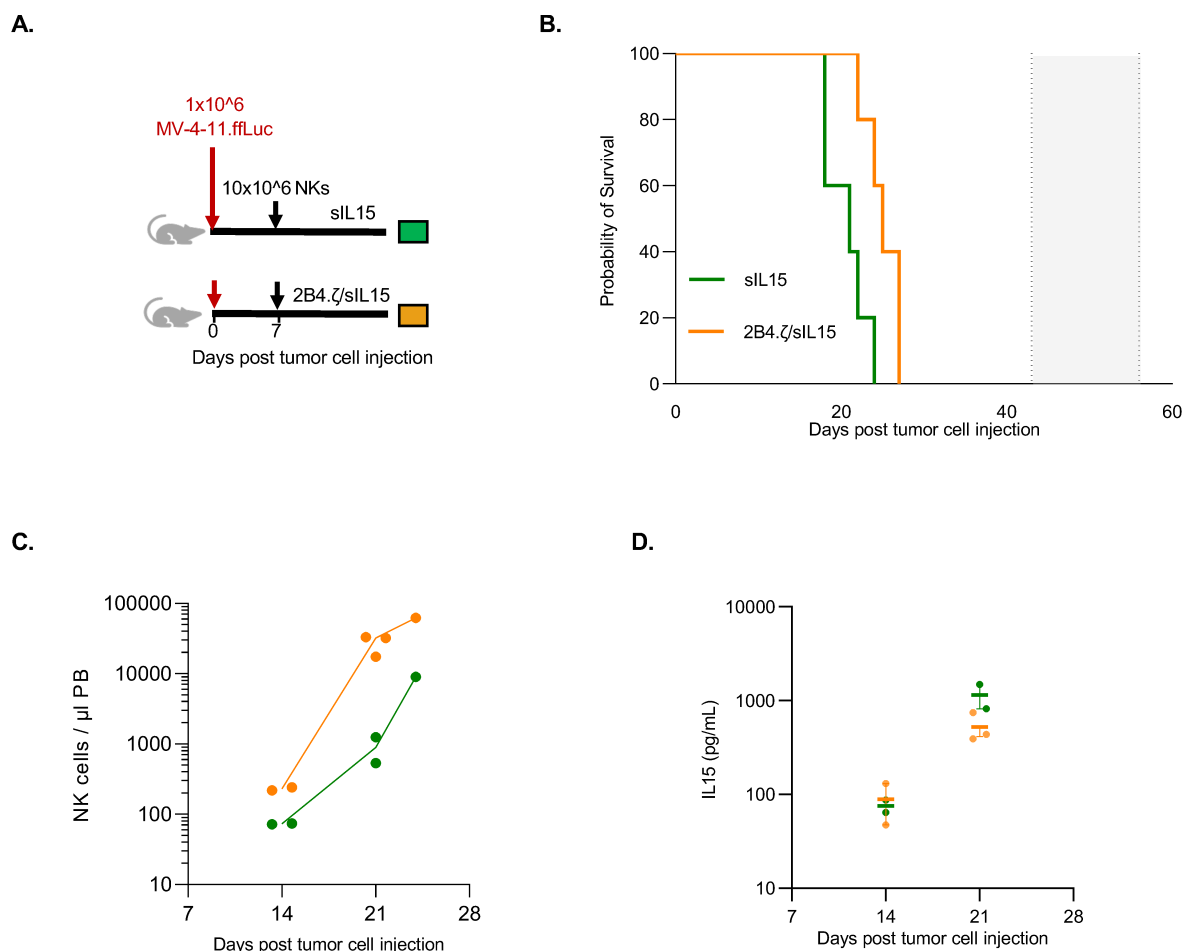
Supplemental Figure 14. IL15 stimulated NK cells promote lethal toxicity of MV-4-11 engrafted mice. (**A**) Schematic of MV-4-11 xenograft treated with IL15-secreting NK cells. On day 0, NSG mice were injected via tail vein with 1×10^6 CD123(+) MV-4-11 cells. In treatment groups (2B4.z/sIL15 or sIL15), 10×10^6 NK cells were administered on day 7. (**B**) Kaplan–Meier survival analysis of MV-4-11 xenografts (n=5 mice each group). Dotted lines border grey shading representing usual survival window of MV-4-11 xenograft model. (**C**) Mouse peripheral blood (PB) was collected at indicated time points and analyzed via flow cytometry. NK cell numbers per microliter of mouse PB were tracked starting on day 14 of the experiment. Each dot represents cell numbers from a single mouse. (**D**) Human IL15 from peripheral blood of MV-4-11 engrafted mice at the indicated time points was quantified (pg/mL) with ELISA (mean +/- SEM, each dot representative of a single mouse).

Supplemental material

BMJ Publishing Group Limited (BMJ) disclaims all liability and responsibility arising from any reliance placed on this supplemental material which has been supplied by the author(s)

J Immunother Cancer

Supplemental Figure 15. IL15 stimulation promotes NK cell expansion and inflammation *in vivo.* (**A**) FACS plots of hCD45(+) cells in the peripheral blood, bone marrow, and spleen of mice at necropsy. hCD45(+)CD33(-)GFP(-) cells: NK cells (blue). Percentage of cells populating NK or AML gates indicated. (**B**) Percentage (%) cell populations in spleen and bone marrow at necropsy (n=3 mice). Mean +/- SEM. (**C**) Human TNFα, (**D**) mouse IL1β and (**E**) mouse IL6 from peripheral blood of MV-4-11 engrafted mice drawn at necropsy and quantified with ELISA. Each dot derived from a single mouse. Mean +/- SEM.
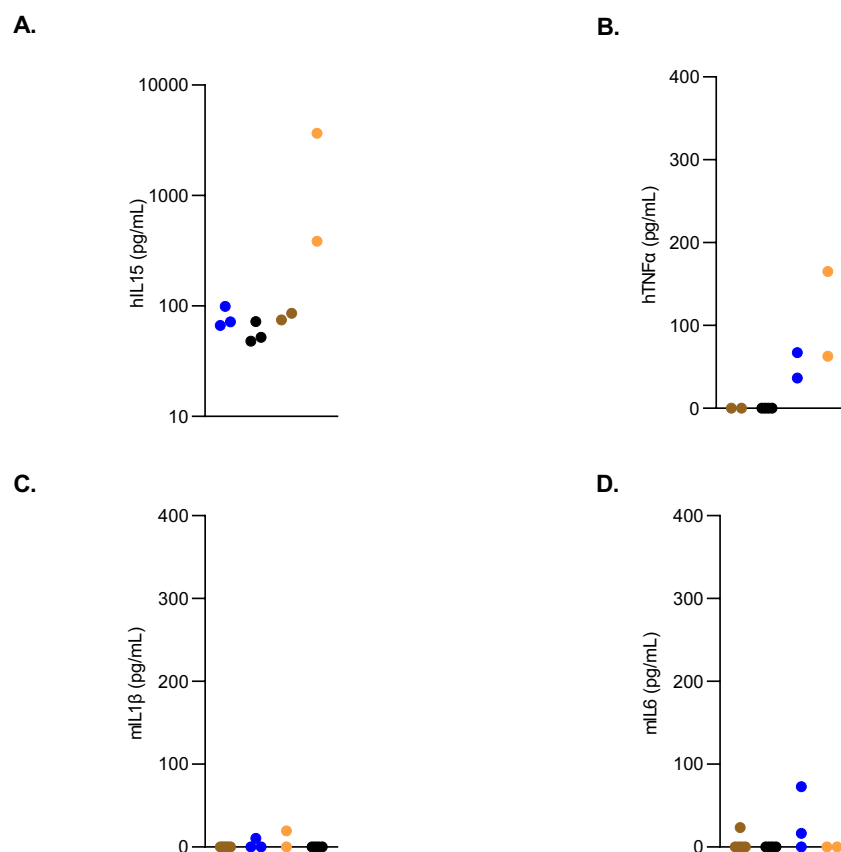
Supplemental Figure 16. IL15-secreting CAR-NK cell treatment promotes inflammation in MOLM-13 engrafted mice. (**A**) Human IL15, (**B**) human TNFα, (**C**) mouse IL1β and (**D**) mouse IL6 analysis from the peripheral blood drawn at necropsy from MOLM-13 engrafted mice. Cytokine measurement (pg/mL) with ELISA. Each dot represents data from a single mouse. n=2-5 mice.

Supplemental material

BMJ Publishing Group Limited (BMJ) disclaims all liability and responsibility arising from any reliance placed on this supplemental material which has been supplied by the author(s)

J Immunother Cancer

Engineering CAR-NK cells to secrete IL15 sustains their anti-AML functionality, but is associated with systemic toxicities
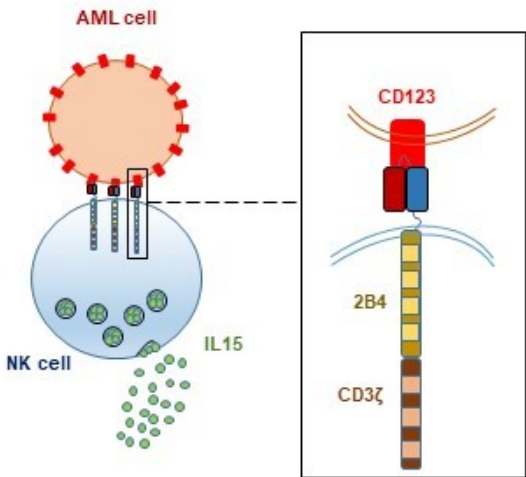
Authors

Ilias Christodoulou, Won Jin Ho, Andrew Marple, Jonas W. Ravich, Ada Tam, Ruyan Rahnama, Adam Fearnow, Cambrynne Rietberg, Sean Yanik, Elena E. Solomou, Ravi Varadhan, Michael A. Koldobskiy, Challice L. Bonifant
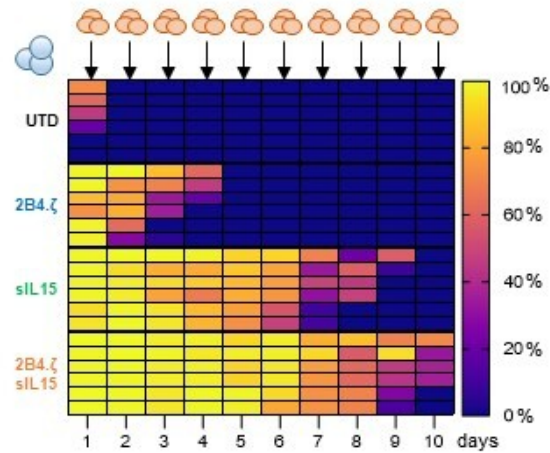
Correspondence

cbonifa2@jh.edu

In Brief

Secretion of IL15 from anti-CD123.2B4.CD3ζ CAR-NK cells enhances their activation and killing potential against Acute Myelogenous Leukemia, but carries the risk of severe systemic toxicity.

sIL15 maintains an activated NK cell phenotype
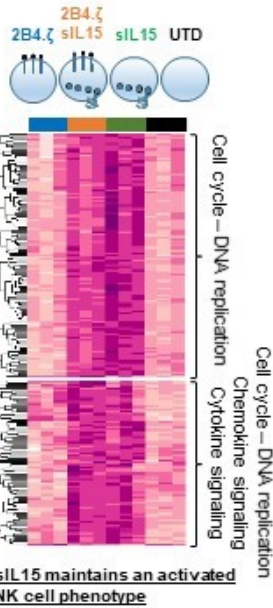
CAR-NK cells secreting IL15 demonstrate sustained and powerful anti-AML cytotoxicity